



저작자표시-비영리-변경금지 2.0 대한민국

이용자는 아래의 조건을 따르는 경우에 한하여 자유롭게

- 이 저작물을 복제, 배포, 전송, 전시, 공연 및 방송할 수 있습니다.

다음과 같은 조건을 따라야 합니다:



저작자표시. 귀하는 원저작자를 표시하여야 합니다.



비영리. 귀하는 이 저작물을 영리 목적으로 이용할 수 없습니다.



변경금지. 귀하는 이 저작물을 개작, 변형 또는 가공할 수 없습니다.

- 귀하는, 이 저작물의 재이용이나 배포의 경우, 이 저작물에 적용된 이용허락조건을 명확하게 나타내어야 합니다.
- 저작권자로부터 별도의 허가를 받으면 이러한 조건들은 적용되지 않습니다.

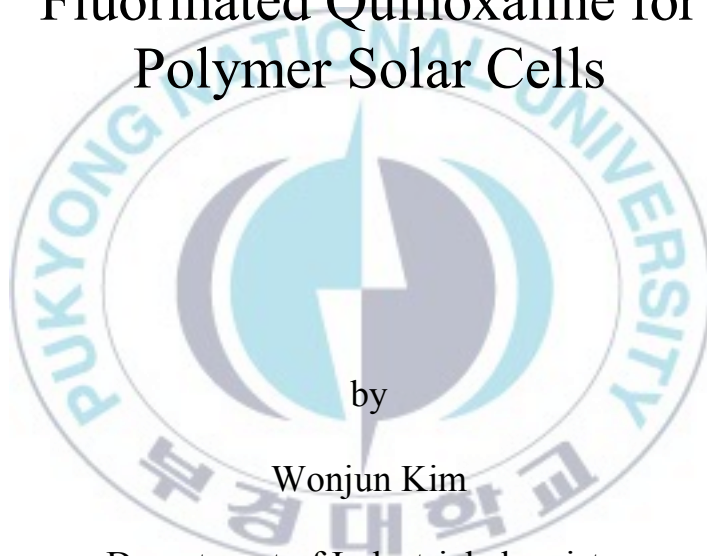
저작권법에 따른 이용자의 권리는 위의 내용에 의하여 영향을 받지 않습니다.

이것은 [이용허락규약\(Legal Code\)](#)을 이해하기 쉽게 요약한 것입니다.

[Disclaimer](#)

Thesis for the Degree of Master of Engineering

Synthesis and Characterization of Alternating  
D-A type Conjugated Polymer Containing  
Fluorinated Quinoxaline for  
Polymer Solar Cells



by

Wonjun Kim

Department of Industrial chemistry

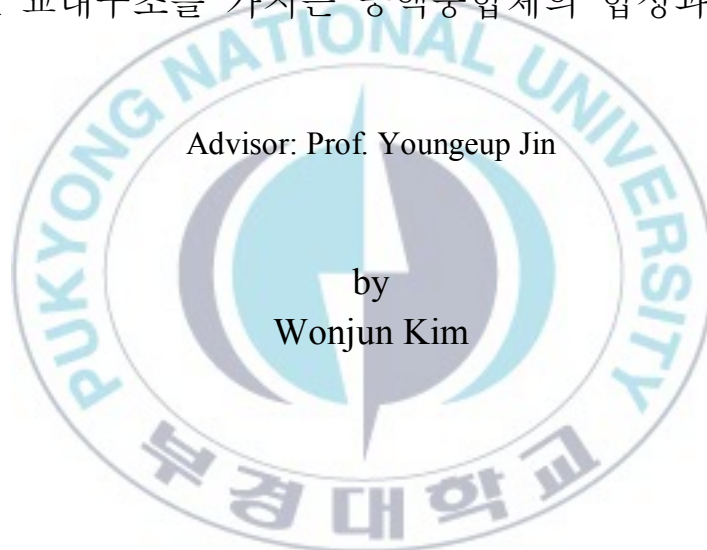
The Graduate School

Pukyong National University

February 2015

# Synthesis and Characterization of Alternating D-A type Conjugated Polymer Containing Fluorinated Quinoxaline for Polymer Solar Cells

(고분자태양전지를 위한 Fluorinated Quinoxaline 을 포함하는  
D-A 교대구조를 가지는 공액중합체의 합성과 특성)



Advisor: Prof. Youngeup Jin

by  
Wonjun Kim

A thesis submitted in partial fulfillment of the requirements  
for the degree of

Master of Engineering

in Department of Industrial Chemistry, The Graduate School,  
Pukyong National University

February 2015

Synthesis and Characterization of Alternating D-A type  
Conjugated Polymer Containing Fluorinated  
Quinoxaline for Polymer Solar Cells

A dissertation

by

Wonjun Kim

Approved by:

---

(Seong Soo Park)

---

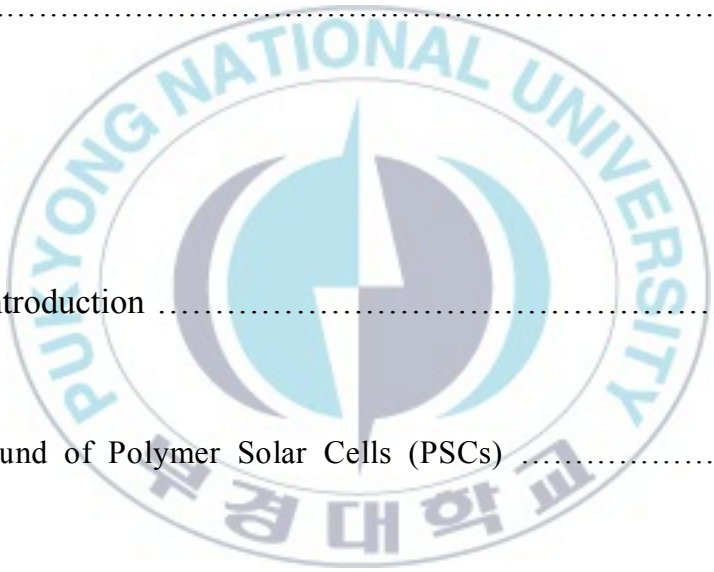
(Dong Wook Jang )

---

(Youngeup Jin)

February 27, 2015

## Contents

Contents .....	i
List of Figures .....	vii
List of Tables .....	x
List of Schemes .....	xi
Abstract .....	xii
	
Chapter I. Introduction .....	1
I-1. Background of Polymer Solar Cells (PSCs) .....	1
I-2. Operating Principles of PSCs .....	3
I-3. Device Structures of PSC .....	4
I-3-1. Bilayer Devices .....	4
I-3-2. Bulk Heterojunction Devices .....	4

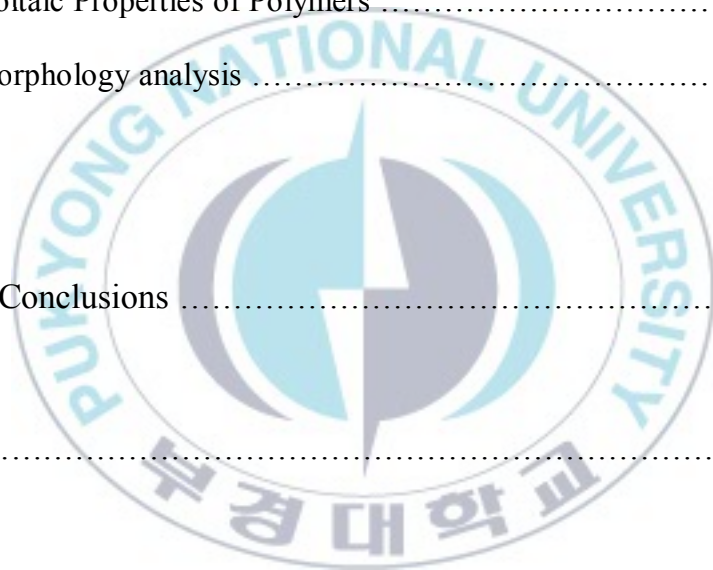
I-4. Parameters of PSCs .....	7
I-4-1. Open-Circuit Voltage ( $V_{oc}$ ) .....	7
I-4-2. Short-Circuit Current Density ( $J_{sc}$ ) .....	8
I-4-3. Fill Factor (FF) .....	9
I-4-4. Requirements for Materials in PSCs .....	9
I-5. Strategies to Synthesize Conjugated Polymers for High Performance .....	10
I-5-1. Donor-Acceptor (D-A) Alternating Structure .....	10
I-5-1-1. Selection of Donor Unit in Conjugated Polymer .....	13
I-5-1-2. Selection of Acceptor Unit in Conjugated Polymer .....	13
I-5-2. Effects of Substitution Introduced in Conjugated Backbone .....	15
I-6. General Method for Synthesis of Conjugated Polymers .....	16
Chapter II. Experimental .....	18
II-1. Materials and Instruments .....	18

II-2. Synthesis of monomers .....	20
II-2-1. Synthesis of donor monomers .....	20
II-2-1-1. Synthesis of 2,5-bis(trimethylstannyl)thiophene .....	20
II-2-1-2. Synthesis of thiophene-3-carbonyl chloride .....	20
II-2-1-3. Synthesis of <i>N,N</i> -diethylthiophene-3-carboxamide .....	21
II-2-1-4. Synthesis of benzo[1,2- <i>b</i> :4,5- <i>b'</i> ]dithiophene-4,8-dione .....	22
II-2-1-5. Synthesis of 4,8-bis(2-ethylhexyloxy)benzo[1,2- <i>b</i> :4,5- <i>b'</i> ]dithiophene .....	22
II-2-1-6. Synthesis of 2,6-bis(trimethyltin)-4,8-bis(2-ethylhexyloxy)benzo[1,2- <i>b</i> :3,4- <i>b'</i> ]dithiophene .....	23
II-2-2. Synthesis of acceptor monomers .....	25
II-2-2-1. Synthesis of 2,3-difluoro-1,4-bis-(trimethylsilyl)benzene .....	25
II-2-2-2. Synthesis of 1,4-dibromo-2,3-difluoro-benzene .....	25
II-2-2-3. Synthesis of 1,4-dibromo-2,3-difluoro-5,6-dinitro-benzene .....	26
II-2-2-4. Synthesis of 3,6-dibromo-4,5-difluorobenzene-1,2-diamine .....	26
II-2-2-5. Synthesis of hexacosane-13,14-dione .....	27
II-2-2-6. Synthesis of 5,8-dibromo-6,7-difluoro-2,3-didodecylquinoxaline .....	28

II-2-2-7. Synthesis of 2,5-dibromo-4-fluoro-nitrobenzene .....	30
II-2-2-8. Synthesis of Synthesis of <i>N</i> -(2',5'-dibromo-4'-fluorophenyl)-2,2,2-trifluoroacetamide .....	30
II-2-2-9. Synthesis of <i>N</i> -(2',5'-dibromo-4'-fluoro-6'-nitrophenyl)-2,2,2-trifluoroacetamide .....	31
II-2-2-10. Synthesis of 2,5-dibromo-4-fluoro-6-nitroaniline .....	31
II-2-2-11. Synthesis of 2,5-dibromo-4-fluoro-5,6-benzenediamine .....	32
II-2-2-12. Synthesis of 5,8-dibromo-2,3-didodecyl-6-fluoroquinoxaline .....	32
II-2-2-13. Synthesis of tributyl(thiophen-2-yl)stannane .....	35
II-2-2-14. Synthesis of 2,3-didodecyl-6,7-difluoro-5,8-di(thiophen-2-yl)quinoxaline .....	35
II-2-2-15. Synthesis of 5,8-bis(5-bromothiophen-2-yl)-2,3-didodecyl-6,7-difluoroquinoxaline .....	36
II-2-2-16. Synthesis of 2,3-didodecyl-6-fluoro-5,8-di(thiophen-2-yl)quinoxaline .....	36
II-2-2-17. Synthesis of 5,8-bis(5-bromothiophen-2-yl)-2,3-didodecyl-6-fluoroquinoxaline .....	37

II-3. Synthesis of polymers .....	39
II-3-1. Synthesis of poly[2,3-didodecyl-6,7-difluoro-5-(thiophen-2-yl)quinoxaline] (YJ-20) .....	39
II-3-2. Synthesis of poly[2,3-didodecyl-7-fluoro-5-(thiophen-2-yl)quinoxaline] (YJ-21) .....	41
II-3-3. Synthesis of poly[5-(4,8-bis((2-ethylhexyl)oxy)benzo[1,2- <i>b</i> :4,5- <i>b'</i> ]dithiophen-2-yl)-2,3-didodecyl-6,7-difluoroquinoxaline] (YJ-22) .....	43
II-3-4. Synthesis of poly[5-(4,8-bis((2-ethylhexyl)oxy)benzo[1,2- <i>b</i> :4,5- <i>b'</i> ]dithiophen-2-yl)-2,3-didodecyl-7-fluoroquinoxaline] (YJ-23) .....	45
II-3-5. Synthesis of poly[5-(5-(4,8-bis((2-ethylhexyl)oxy)benzo[1,2- <i>b</i> :4,5- <i>b'</i> ]dithiophen-2-yl)thiophen-2-yl)-2,3-didodecyl-6,7-difluoro-8-(thiophen- 2-yl)quinoxaline] (YJ-24) .....	47
II-3-6. Synthesis of poly[8-(5-(4,8-bis((2-ethylhexyl)oxy)benzo[1,2- <i>b</i> :4,5- <i>b'</i> ]dithiophen-2-yl)thiophen-2-yl)-2,3-didodecyl-6-fluoro-5-(thiophen-2- yl)quinoxaline] (YJ-25) .....	49

Chapter III. Results and Discussion .....	51
III-1. Polymerization results .....	51
III-2. Optical Properties of Polymers .....	53
III-3. Electrochemical Properties of Polymers .....	59
III-4. Photovoltaic Properties of Polymers .....	61
III-5. Film morphology analysis .....	67
Chapter IV. Conclusions .....	70
References .....	72



## List of Figures

Figure 1-1. Representative materials of PSCs.

Figure 1-2. Working mechanism for donor-acceptor heterojunction solar cells.

Figure 1-3. Structures of (a) bilayer device and (b) bulk heterojunction device.

Figure I-4. Molecular orbital interactions of donor and acceptor units, resulting in a narrowing of the band gap in D-A conjugated copolymers.

Figure I-5. Catalytic cycle of transition-metal-catalyzed reactions.

Figure III-2. Thermo gravimetric analysis of polymers.

Figure III-2. UV-visible absorption spectra of polymers in o-dichlorobenzene solution.

Figure III-3. UV-visible absorption spectra of polymers in a thin film formed via spin-cast from a solution in o-dichlorobenzene.

Figure III-4. UV-visible absorption spectra of YJ-20(red) and YJ-21(blue) in o-dichlorobenzene solution.

Figure III-5. UV-visible absorption spectra of YJ-20(red) and YJ-21(blue) in a thin film formed via spin-cast from a solution in o-dichlorobenzene (1wt%).

Figure III-6. UV-visible absorption spectra of YJ-22(orange) and YJ-23(green) in o-dichlorobenzene solution.

Figure III-7. UV-visible absorption spectra of YJ-22(orange) and YJ-23(green) in a thin film formed via spin-cast from a solution in o-dichlorobenzene (1wt%).

Figure III-8. UV-visible absorption spectra of YJ-24(pink) and YJ-25(purple) in o-dichlorobenzene solution.

Figure III-9. UV-visible absorption spectra of YJ-24(pink) and YJ-25(purple) in a thin film formed via spin-cast from a solution in o-dichlorobenzene (1wt%).

Figure III-10. Cyclic voltammetry curves of the polymers in 0.1 M  $\text{Bu}_4\text{NPF}_6$  acetonitrile solution at a scan rate of 100 mV/s at room temperature (vs an Ag quasi-reference electrode).

Figure III-11. (a) J-V characteristics of the device based on YJ-20:PCBM blend and (b) YJ-21:PCBM blend.

Figure III-12. (a) J-V characteristics of the device based on YJ-22:PCBM blend and (b) YJ-23:PCBM blend.

Figure III-13. (a) J-V characteristics of the device based on YJ-24:PCBM blend and  
(b) YJ-25:PCBM blend.

Figure III-14. J-V characteristics of the device based on YJ-24:PC<sub>70</sub>BM (1:1.5)  
blend with 3 vol% DIO.

Figure III-15. AFM topography images of films spin coated from YJ-24:PC<sub>70</sub>BM  
(1:2) using chlorobenzene without additives (a) and without DIO (b),  
using 1,2-dichlorobenzene without additives (c) and with DIO (d).  
The scan size of the images is 2  $\mu\text{m} \times 2 \mu\text{m}$ .

Figure III-16. AFM phase images of films spin coated from YJ-24:PC<sub>70</sub>BM (1:2)  
using chlorobenzene without additives (a) and with DIO (b), using  
1,2-dichlorobenzene without additives (c) and with DIO (d). The scan  
size of the images is 2  $\mu\text{m} \times 2 \mu\text{m}$ .

## List of Tables

Table III-1. Polymerization results.

Table III-2. Decomposition temperatures of polymers.

Table III-3. Optical properties of polymers.

Table III-4. Electrochemical properties of the polymers.

Table III-5. Photovoltaic performance of devices based on YJ-20 or YJ-21.

Table III-6. Photovoltaic performance of devices based on YJ-22 or YJ-23.

Table III-7. Photovoltaic performance of devices based on YJ-24 or YJ-25.

Table III-8. Photovoltaic performance of devices based on YJ-24:PC<sub>70</sub>BM with additive.

## List of Schemes

Scheme 1. Synthetic route of donor monomers.

Scheme 2. Synthetic route of difluoroquinoxaline (DFQ<sub>x</sub>).

Scheme 3. Synthetic route of monofluoroquinoxaline (FQ<sub>x</sub>).

Scheme 4. Synthetic route of di(thiophenyl)quinoxalines (DTDFQ<sub>x</sub>, DTFQ<sub>x</sub>).

Scheme 5. Synthetic route of PTDFQ<sub>x</sub> (YJ-20).

Scheme 6. Synthetic route of PTFQ<sub>x</sub> (YJ-21).

Scheme 7. Synthetic route of PBDTDFQ<sub>x</sub> (YJ-22).

Scheme 8. Synthetic route of PBDTFQ<sub>x</sub> (YJ-23).

Scheme 9. Synthetic route of PBDTDTDFQ<sub>x</sub> (YJ-24).

Scheme 10. Synthetic route of PBDTDTFQ<sub>x</sub> (YJ-25).

고분자태양전지를 위한 Fluorinated Quinoxaline 을 포함하는  
D-A 교대구조를 가지는 공액중합체의 합성과 특성

김원준

부경대학교 대학원 공업화학과

요 약

고분자 태양전지는 유연성을 가질 수 있고, 저가격 대면적의 용액공정을 할 수 있다는 장점을 가지고 있어 대체 에너지원으로 고려되어 많은 연구가 진행되고 있다. 최근 연구에서 단일층의 bulkheterojunction(BHJ) 고분자 태양전지의 효율은 8% 이상까지 보고되었다. 고 효율을 나타내는 태양전지에서 고분자는 빛의 흡수량을 늘리기 위해 좁은 밴드갭을 가져야 하며, 효과적인 전하분리를 위해 acceptor물질과 에너지레벨의 차이가 적당해야 하고, 분자 내 전하이동을 높이기 위해 donor-acceptor(D-A)구조의 고분자를 합성해야 한다.

본 연구에서는 액티브레이어에서 electron-acceptor로 가장 많이 사용되고 있는 BT와 유사한 구조를 가지는 quinoxaline에 치환기로 fluorine을 1개 또는 2개를 도입하였고 solubility를 증가시키기 위해 2개의 dodecyl기를 도입한 새로운 acceptor 단량체를 디자인하였고, 그를 포함하는 새로운 고분자를 합성하였다. 이를 통해 fluorine이 가지는 electron-withdrawing 효과가 태양전지에 나타나는 특성변화를 관찰하였다.

## **Chapter I. Introduction**

### **I-1. Background of Polymer Solar Cells (PSCs)**

Recently, exhaustion of energy is emerging as a major issue. Using solar energy can be right way to solve this issue. Inorganic photovoltaic technology has not been practical because of its limitation, such as high material and manufacturing costs. Compared with inorganic solar cells, polymer solar cells(PSCs) have attracted attention due to their advantages, including of light weight, large area and low cost according to application of solution process.

Another crucial advantage of polymer solar cells is the variety of the polymer structures in organic chemistry, where quite a number of combinations of various backbones are available. So properties of the resulting polymers, such as solubility, carrier mobility and energy levels for photovoltaic applications can be easily tuned by changing components in polymer backbone.

Devices of PSCs changed from homopolymer single cells to bilayer heterojunction cells and bulk heterojunction cells are mainly used in recent years.

In bulk hetero-junction (BHJ) polymer solar cells, conjugated polymer as electron-donor (D) and PCBM derivatives as electron-acceptor (A) materials are blended to provide the photoactive layer.

According to development of that, Power conversion efficiency (PCE) could be

significantly increased, but was still insufficient to be commercialized.

Some successful ways to enhance PCE have been reported by researcher.

These ways are

1. Synthesis of low band gap polymer to improve light harvesting
2. Utilization of some additives to improve phase separation of active layer in BHJ devices
3. Enhancing planarity of polymer backbone to increase  $\pi$ - $\pi$  interaction.
4. Introducing donor-acceptor (D-A) alternating structure into polymer backbone to increase intramolecular charge transfer (ICT) from an electron-rich unit to an electron-deficient unit,
5. Production of tandem solar cell devices to broaden light absorption spectra.

In consequence of these researches, PCE was reported over 8% in single cells and over 10% in tandem cells recently.

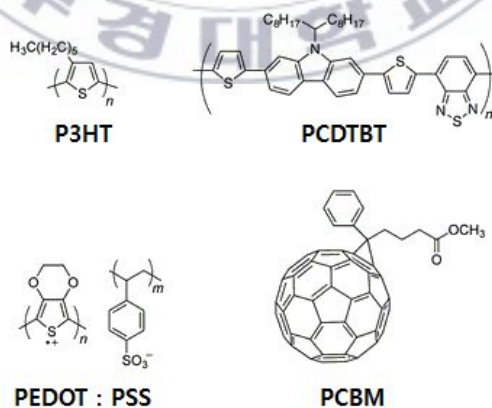


**Figure I-1.** Representative materials of PSCs.

## I-2. Operating Principles of PSCs

As shown in Figure I-2, the general operating principle in the donor-acceptor heterojunction solar cells first involves the photoexcitation of the donor material by the absorption of light energy to form excitons. These excitons, coulomb-correlated electron-hole pairs, diffuse to the donor-acceptor (D-A) interface where exciton dissociation occurs via an electron-transfer process. The fully separated free charge carriers transport to the respective electrodes in the opposite direction with the aid of the internal electric field, which in turn generates the photocurrent and photovoltage.

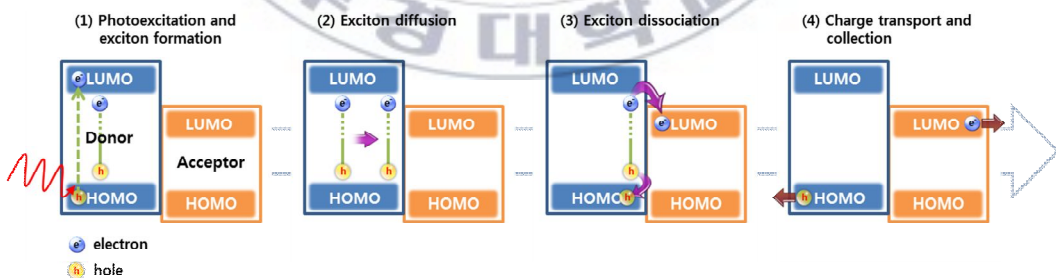


**Figure I-2.** Working mechanism for donor-acceptor heterojunction solar cells.

### **I-3. Device Structures of PSCs**

#### **I-3-1. Bilayer Devices**

In a bilayer heterojunction device (Figure I-3a), p-type and n-type semiconductors are sequentially arranged on top of each layer. Such bilayer devices involving organic semiconductors were introduced with variety material combinations.<sup>6-14</sup> In such devices, only excitons formed within 10-20 nm distance from the interface can reach the interface between p-type and n-type semiconductors. Other excitons, created in the volume over 20 nm away from the interface, lead to the loss of photons and that results in low quantum efficiencies.<sup>15</sup> Because efficiency of bilayer solar cells is limited by the charge generation 10-20 nm around the donor-acceptor interface, using thicker films produce optical filter effects of the absorbing material before the light gets to the interface. As a result, that cause a minimum photocurrent at the maximum of the optical absorption spectrum.<sup>16</sup> Also, the film thicknesses have to be optimized for the interference effects in the multiple stacked thin film structure.<sup>17,18</sup>

#### **I-3-2. Bulk Heterojunction Devices**

Bulk heterojunction (BHJ) devices contain a photoactive layer blended with the donor and acceptor components (Figure I-3b). BHJ devices provide wide

interfacial area and it lead to more efficient charge separation because charge separation is performed in surface between donor polymer and acceptor domain. Therefore, sharply designed morphology (the donor-acceptor phase separation) plays a critical role to achieve suitable charge transfer in the BHJ devices. When Figuration of the morphology was similar to a 10~20 nm nanoscale interpenetrating network, PSCs empirically achieved a high performance.<sup>19</sup> In such a nanoscale interpenetrating network, each interface is within a distance less than the exciton diffusion length (~10 nm) from the place where chromophore absorbs the light. While in the bilayer cells the donor and acceptor phases are manifestly separated from each other and can be selectively connected to the anode and cathode, the bulk heterojunction solar cells include a single layer blending both phases.<sup>19</sup> There is no fixed direction for the internal fields of separated charges; that is, the electrons and holes have no steady direction they should move.<sup>19</sup> Therefore, a symmetry breaking condition (like using different work-function electrodes) is necessary in bulk heterojunctions. Otherwise, only the difference between work functions of each electrodes can act as driving force. Furthermore, separated charges require percolated pathways for the hole and electron transporting phases to the contacts. In other words, the donor and acceptor phases have to form specific morphology of a nanoscale, bicontinuous, and interpenetrating network.<sup>20</sup> Therefore, the bulk heterojunction devices are much more sensitive to the nanoscale morphology in the blend. Bulk

heterojunctions can be achieved by co-deposition of donor and acceptor pigments<sup>21-24</sup> or solution casting of either polymer/polymer,<sup>14,25,26</sup> polymer/molecule,<sup>7,19,27</sup> or molecule/molecule<sup>28,29</sup> donor-acceptor blends.<sup>26,30</sup>

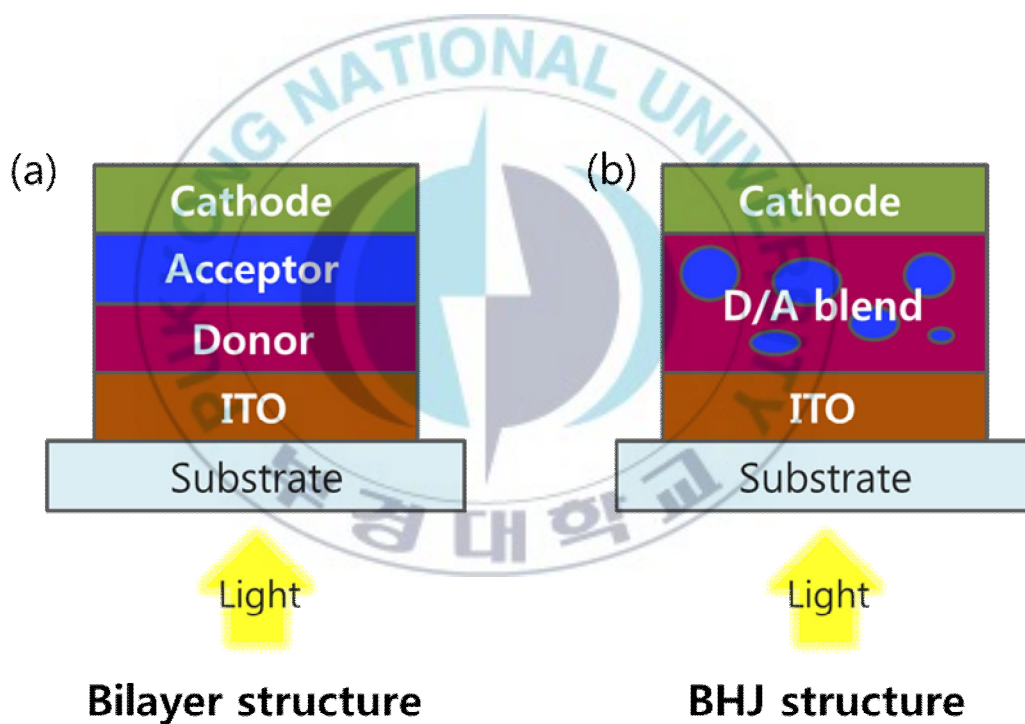


**Figure I-3.** Structures of (a) bilayer device and (b) bulk hetero junction device.

## I-4. Parameters of PSCs

To design ideal donor polymers in BHJ solar cells with high power conversion efficiency ( $PCE = V_{oc} \times J_{sc} \times FF / P_{in}$ ), the following issues need to be carefully addressed.

### I-4-1. Open-Circuit Voltage ( $V_{oc}$ )

$V_{oc}$  is closely related to the difference between the HOMO level of the donor polymer and the LUMO level of the acceptor.<sup>31</sup> Using the polymers with low-lying HOMO levels could achieve higher  $V_{oc}$ . However, the donor polymer with extremely low HOMO level would not be effective. This is because generally a minimum energy difference of  $\sim 0.3$  eV between the LUMO energy levels of the donor polymer and the acceptor is required to facilitate efficient exciton dissociation and charge separation. Continuously lowering the HOMO level of the donor polymer would enlarge the band gap of the polymer, decreasing the light absorbing ability of the donor polymer (thereby a low  $J_{sc}$ ). The origin of  $V_{oc}$  is still under intense debate, and recent data indicate that  $V_{oc}$  is decided by a couple of other factors besides just the HOMO level of the polymer.<sup>32,33</sup> Furthermore, figuration of side chains, intermolecular distances, and morphology of active layer have also been demonstrated to have a remarkable effect on the  $V_{oc}$ .<sup>34</sup>

#### I-4-2. Short-Circuit Current Density ( $J_{sc}$ )

The theoretical upper limit for  $J_{sc}$  of any polymer solar cell is decided by the number of excitons created during solar illumination. Ideally, the absorption of the active layer should be compatible with the solar spectrum to maximize the exciton generation. Since PCBM has a poor absorption in the visible and near-IR region where most of the solar flux is located, the donor polymer is key factor in a mechanism of light absorption. Approximately 70% of the sunlight energy is concentrated on the wavelength range from 380 to 900 nm,<sup>35</sup> for this reason, an ideal polymer should be equipped with a broad and strong absorption spectra in this region, which requires a band gap of the polymer to adjust 1.4 ~ 1.5 eV. A narrower band gap polymer could absorb more light, which would enhance the  $J_{sc}$ ; however, continuously lowering the band gap necessarily results in high HOMO level of the donor polymer. the HOMO level of the donor polymer would be increased to show excessively low the band gap (since it would be not good that the difference of LUMO level between donor polymer and acceptor would be over 0.3 eV for efficient exciton dissociation and charge separation)<sup>36</sup> and would reduce the  $V_{oc}$ . the actual  $J_{sc}$  measured from a polymer solar cell is usually significantly lower than the theoretical  $J_{sc}$  due to a number of loss mechanisms (e.g., monomolecular or bimolecular recombination) during the charge generation, transport, and collection.<sup>35,37</sup> Therefore the PSCs should gratify various requirements to reduce these losses, such as high molecular weight, high

charge mobility, and optimized morphology of photoactive layer, all of which will contribute to enhancing the actual  $J_{sc}$ .

### **I-4-3. Fill Factor (FF)**

Fill factor (FF) is a relatively unknown parameter among the three. The FF is the ratio between the maximum obtainable power and the product of  $J_{sc}$  and  $V_{oc}$ . Many factors could affect it, such as charge carrier mobility and balance, interface recombination, series and shunt resistances, film morphology and miscibility between the donor and acceptor. In point of material development, planarity of backbone, intermolecular interaction, molecular packing and crystallinity are also closely related to FF. these conditions can be tuned by Side-chain selection. Side-chain executes a role optimizing  $\pi$ -stacking, polymer crystallinity and material miscibility, by controlling steric hindrance of polymer backbone. However, it is necessary to definitize the relation between FF and PSCs for development of PSCs.

### **I-4-4. Requirements for Materials in PSCs**

As explained above, it would be important to have a high value of fill factor, external quantum efficiency and optimized morphology. If PSCs have a fill factor of 0.65, an external quantum efficiency of 65% and an optimized morphology in polymer:PCBM BHJ solar cell, it is shown that a PCE of 10% can be achieved by

an “ideal” polymer with an band gap of 1.5 eV and a HOMO level around -5.4 eV. Though the experimentally determined  $V_{oc}$  can be very close to the predicted value based on the measured HOMO level of the polymer.

Finally, besides high PCE, availability of solution process (side chains effects) and long-term stability of polymer solar cells (related with both materials and encapsulation) are of equal importance for future application and commercialization. In short, the properties desired for a high performance polymer are (1) good solubility, (2) high molecular weight, (3) HOMO level around -5.4 eV, (4) LUMO level around -3.9 eV, (5) high hole mobility, (6) optimal morphology, and (7) long-term stability.

## **I-5. Strategies to Synthesize Conjugated Polymers for High Performance.**

### **I-5-1. Donor-Acceptor (D-A) Alternating Structure**

Donor-acceptor (D-A) alternating conjugated polymers were extensively developed and have been most commonly used as donor materials for PSCs because their characteristic optical and electronic properties, such as light-absorption ability and energy levels, can be tuned easily by controlling the intramolecular charge transfer (ICT) from donor unit to acceptor unit. Recently, a

PCE over 7 % is frequently reported in the field of BHJ solar cells, largely due to the successful development of D-A alternating conjugated polymers.<sup>38-42</sup> The principle of band gap and energy level control by ICT interaction in D-A alternating conjugated polymers can be easily explained by molecular orbital theory. As shown in Figure I-4, the HOMO of the donor unit will generate two new occupied molecular orbitals after covalent bond connection of two different moieties by interacting with that of the acceptor unit, one of them is higher and the other one is lower than the two initial HOMOs before molecular orbital hybridization. Two new unoccupied molecular orbitals would also be generated in a similar manner after molecular orbital hybridization, where one is lower and the other is higher than the two initial LUMOs of the two moieties. Hence, the overall effect of this redistribution of frontier molecular orbitals is the formation of a higher-positioned HOMO and a lower-positioned LUMO in the whole conjugated main chain, and this accordingly leads to the narrowing of the band gap. Clearly, the rational selection of building blocks, including both donor units and acceptor units is critical to the realization of the well-defined control of the photophysical properties and frontier molecular orbital energy levels of the resulting copolymers to meet the requirements for BHJ-PSC applications. Therefore, various aromatic heterocycles were used as building blocks to develop highly efficient donor polymers for BHJ solar cell applications based on the D-A alternating design. Moreover, the fine tuning of the structure (such as introduction of functional

groups onto the backbone, the selection of alkyl side chains, and end capping, etc.) is also critical for obtaining high-performing donor polymers, although the conjugated backbone mainly determined the intrinsic electronic properties (especially band gaps, energy levels, and charge carrier transporting ability). It should be pointed out that conjugated polymers which consist of alternating electron-rich building blocks but can provide stable quinoidal structures are another class of state-of-the-art donor polymers for BHJ-PSCs, apart from D-A conjugated polymers.<sup>43,44</sup> BHJ-PSCs based on this kind of material even reached PCEs higher than 8.0% after optimization of device.<sup>45</sup>

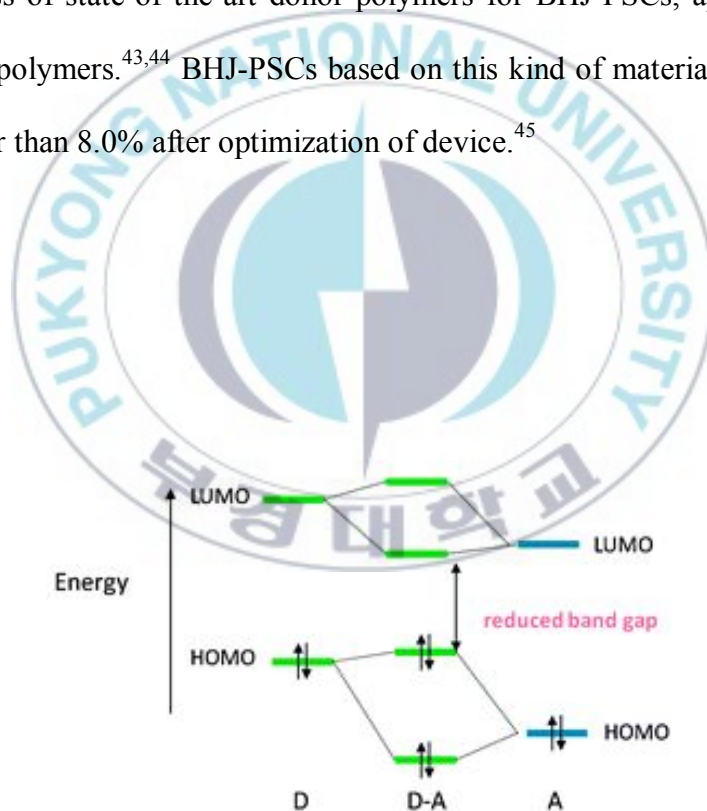


**Figure I-4.** Molecular orbital interactions of donor and acceptor units, resulting in a narrowing of the band gap in D-A conjugated copolymers.

### **I-5-1-1. Selection of Donor Unit in Conjugated Polymer**

The benzo[1,2-*b*:4,5-*b'*]-dithiophene (BDT), recent representative of electron donating units has been at the center of attention as an attractive building block for BHJ solar cells. BDT have a benzene ring in the center and two flanking fused thiophene rings. BDT units offer two advantages: the alkylation (to improve the solubility of resulting polymers) can be practicable on the center benzene ring, and the two flanking thiophene units offer much less steric hindrance with adjacent acceptor units, leading to a more planar backbone. It also has weaker electron-donating ability compared with that of the other donor units. (e.g. thiophene, CPT) Therefore, the HOMO levels of some BDT-based polymers are closer to the ideal HOMO energy level.<sup>39,46-48</sup> Together with a relatively narrow band gap, a few BDT-based polymers have reported PCE over 6% in their BHJ cells. Particularly, BHJ PV devices based on PBDT-DT<sub>f</sub>BT has been shown with a  $V_{oc}$  around 0.9 V and a  $J_{sc}$  over 12 mA/cm<sup>2</sup>, leading to a PCE over 7%

### **I-5-1-2. Selection of Acceptor Unit in Conjugated Polymer**

The most popularly used acceptor unit is the 2,1,3-benzothiadiazole (BT). Because of its strong electron-accepting ability and commercial availability, BT has been the most famous electron accepting building block in low-band-gap conjugated polymers. Moreover, these two N atoms in the thiadiazole ring could possibly form hydrogen bonding with adjacent units (e.g., the hydrogen atom on

the thiophene ring), leading to increased planarity of backbone. With all these merits, many polymers containing a BT unit have shown low band gaps and good photovoltaic performance. Adding one thienyl group on both sides of the BT, it becomes di-2-thienyl-2,1,3-benzothiadiazole (DTBT), which has a few more advantages in comparison with the fundamental BT unit. First, the two flanking thienyl units reduce the otherwise possibly steric hindrance between the BT unit and donor aromatic units (especially when benzene based aromatics are used). Thus, the synthesized donor-acceptor polymers form more planar structures, thereby reducing the band gap by enhancing the D-A conjugation. In addition, a more planar conjugated backbone facilitates the interchain interactions among polymers in the solid state, improving the charge carrier mobility. Second, while the electron-accepting BT unit maintains the low band gap, the two electron-rich, flanking thienyl units would help improve the hole mobility, since thiophene-based polymers (such as P3HT) have shown noticeably high hole mobility.<sup>49</sup> Third, the BT unit has limited positions for addition of solubilizing chains or substituents, and attaching these units would likely introduce steric hindrance. To this end, these flanking thienyl units can provide more possible positions for further modification of electronic properties and solubility of conjugated polymers, with minimal steric hindrance involved if properly introduced.<sup>50</sup> However, due to the electron-rich nature of these thienyl units, in some cases, the two flanking thienyl units slightly increase the HOMO levels of the conjugated

polymers when compared with BT-based polymers.

Quinoxaline (Qx) derived from BT is another promising acceptor unit for constructing D-A alternating conjugated copolymers. The electron-withdrawing capability of Qx is slightly weaker than that of BT, which would lead to slightly larger band gaps for the resulting polymers. Similar to BT, one of the important advantages of quinoxaline is that the low-lying HOMO levels can be maintained for the resulting polymers, which will be beneficial for not only the chemical stability of the polymer but also for obtaining a high  $V_{oc}$  in the resulting devices. Also, Qx can be alkylated to enhance the solubility of polymers without introducing steric hindrance.<sup>51, 52</sup>

### **I-5-2. Effects of Substitution Introduced in Conjugated Backbone**

It is well known that the introduction of an electron-withdrawing group into the polymer backbone can lower its energy levels. (both HOMO and LUMO energy levels) Among various electron-withdrawing groups, fluorine is the smallest group with a van der Waals radius of 1.35 Å and an electronegativity of 4.0. the use of fluorine has been proven to be effective in lowering the HOMO energy level and resulting in higher  $V_{oc}$  and improved performance. Compared to the value of reduced HOMO energy level, the value of decreased LUMO energy level was relatively lesser. The band gap of polymer was consequentially widened for that reason, nevertheless the loss by broadened band gap was so small that the  $J_{sc}$

was hardly affected.

## I-6. General Method for Synthesis of Conjugated Polymers

The construction of conjugated polymers lies essentially in the efficient carbon-carbon single bond formation between two unsaturated carbons in the aromatic units. In addition to electrochemical<sup>53-55</sup> or chemical<sup>56</sup> oxidative polymerizations, transition-metal-catalyzed cross-coupling reactions provide a particularly powerful arsenal for  $Csp^2-Csp^2$  and  $Csp-Csp^2$  bond formation.<sup>57</sup> The reaction, in general, involves a transition-metal-catalyzed oxidative addition reaction across the C-X bond of an electrophile and then transmetalation with a main group organometallic nucleophile, followed by a reductive elimination step leading to the carbon-carbon bond formation. Concomitantly the active catalyst is regenerated (Figure I-4). The most commonly employed transition-metal catalysts are nickel- or palladium based complexes, although other metals have also been used. The organometallic nucleophiles can be Grignard reagents (Kumada-Corriu),<sup>58</sup> stannyl (Stille),<sup>59</sup> boron reagents (Suzuki-Miyaura),<sup>60</sup> or copper (Sonogashira).<sup>61</sup> Thus, conjugation lengths can be extended through consecutive transformations in the catalytic cycle. When the electrophilic and nucleophilic centers of the monomeric substrates are readily accessible, regioselectivity of the

polymers can be easily achieved. Another advantage is that these reaction conditions are generally mild and can tolerate many functional groups. This is particularly important for synthesizing advanced functional conjugated polymers. Stille and Suzuki coupling reactions using two distinct monomers are the most efficient and widely used methods for preparing alternating copolymers. It is noteworthy that stannyl groups substituted on the benzene ring of the monomer substrate always give poor reactivity with aryl halides under Stille coupling conditions.<sup>62</sup> Therefore, Stille coupling is more suitable for thiophene-containing polymers using monomers with stannyl groups on the thiophene ring, whereas Suzuki coupling is more widely used for preparing benzene-containing polymers with boronic groups on the benzene ring of the monomer. On the other hand, nickel-mediated Yamamoto dehalogenation coupling reactions also provide an alternative pathway for carrying out self-polymerization of single monomers.<sup>63</sup>

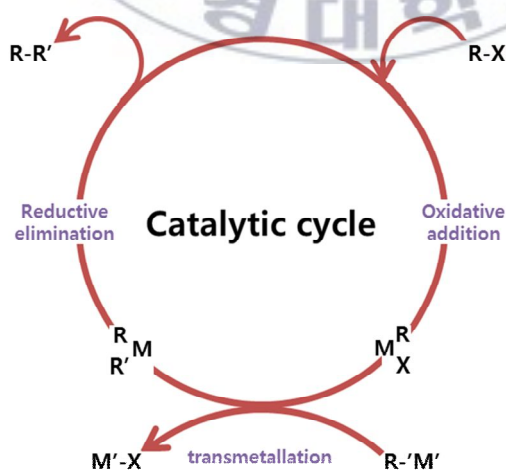


**Figure I-5.** Catalytic cycle of transition-metal-catalyzed reactions

## Chapter II. Experimental

### II-1. Materials and Instruments

All reagents were purchased from Aldrich or TCI, and used without further purification. Solvents were purified by normal procedure and handled under moisture-free atmosphere.  $^1\text{H}$  and  $^{13}\text{C}$  NMR spectra were recorded with a JEOL JNM ECP-400 spectrometer and chemical shifts were recorded in ppm units with TMS as the internal standard. Flash column chromatography was performed with Merck silica gel 60 (particle size 230-400 mesh ASTM) with ethyl acetate / hexane / methylene chloride gradients unless otherwise indicated. Analytical thin layer chromatography (TLC) was conducted using Merck 0.25 mm silica gel 60F pre-coated aluminum plates with fluorescent indicator UV254. High resolution mass spectra (HRMS) were recorded on a JEOL JMS-700 mass spectrometer under electron impact (EI) or fast atom bombardment (FAB) conditions in the Pukyong National University (Busan, Korea). Elemental analyses (EA) were performed by Flash EA 1112 Series. The UV-vis absorption spectra were recorded by a Varian 5E UV/VIS/NIR spectrophotometer. The CV was performed with a solution of tetrabutylammonium hexafluorophosphate ( $\text{Bu}_4\text{NPF}_6$ ; 0.10 M) in acetonitrile at a scan rate of 100 mV/s at room temperature. Pt wire and Ag/AgNO<sub>3</sub> electrode were used as the counter electrode and reference

electrode, respectively. The energy level of the Ag/AgNO<sub>3</sub> reference electrode (calibrated by the FC/FC<sup>+</sup> redox system) was 4.80 eV below the vacuum level. HOMO levels were calculated according to the empirical formula ( $E_{\text{HOMO}} = -([E_{\text{onset}}]_{\text{ox}} + 4.80) \text{ eV}$ ). For the EL experiment, poly(3,4-ethylenedioxythiophene) (PEDOT) doped with poly(styrenesulfonate) (PSS), as the hole-injection-transport layer, was introduced between emissive layer and ITO glass substrate cleaned by successive ultrasonic treatments. The solution of the PEDOT:PSS in aqueous isopropyl alcohol was spin-coated on the surface-treated ITO substrate and dried on a hot plate for 30 min at 110 °C. On top of the PEDOT:PSS layer, the film of photoactive layer was obtained by spin casting o-dichlorobenzene solution blended with polymer and PCBM. The film was dried in vacuum, and aluminum electrodes were deposited on the top of the small molecule films through a mask by vacuum evaporation at pressures below 10<sup>-7</sup>Torr, yielding active areas of 4 mm<sup>2</sup>.

## II-2. Synthesis of Monomers

### II-2-1. Synthesis of Donor Monomers

#### II-2-1-1. Synthesis of 2,5-bis(trimethylstannyl)thiophene (2)

To a solution of 1 g (11.88 mmol) of thiophene in 40 mL of THF at -78 °C under argon was slowly added 27.95 mL (47.52 mmol) of 1.7M *t*-Butyllithium in THF. After 30 min at -78 °C, the reaction mixture was warmed to room temperature, stirred for 1 hr and cooled back to -78 °C. The reaction mixture was added 49.9 mL (49.9 mmol) of 1M trimethyltin chloride. After 30min at -78 °C, the reaction mixture was warmed to room temperature, stirred for overnight, treated with 20 ml of water. The reaction mixture was diluted with ether and washed with water. The organic phase was dried MgSO<sub>4</sub>, and after removal of the solvent under reduced pressure. The crude brown solid was recrystallized from ether/EtOH to give 1.02 g (28%) of compound **28** white solid. <sup>1</sup>H NMR (300 MHz, CDCl<sub>3</sub>) δ 7.37 (s, 2H), 0.34 (s, 18H). <sup>13</sup>C NMR (75 MHz, CDCl<sub>3</sub>) δ 205.39, 136.00, -9.02. HRMS (FAB<sup>+</sup>, m/z) [M]<sup>+</sup> calcd for C<sub>10</sub>H<sub>20</sub>SSn<sub>2</sub> 411.9330, measured 411.9335.

#### II-2-1-2. Synthesis of thiophene-3-carbonyl chloride (4)

Thiophene-3-carboxylic acid (10 g, 78.03 mol) and 100 mL of methylene

chloride were put into a 250 mL flask. The mixture was cooled by ice-water bath, and then oxalyl chloride (78.03 g, 156.07 mol) was added in one portion. The reactant was stirred overnight at ambient temperature, and a clear solution was obtained. After removing the solvent and unreacted oxalyl chloride by rotary evaporation, compound **4** was obtained as white solid. It was dissolved into 100 mL of methylene chloride and used for the next step.

### II-2-1-3. Synthesis of *N,N*-diethylthiophene-3-carboxamide (**5**)

In a 250 mL flask in ice-water bath, 16.15 mL of diethylamine (156.07 mol) and 100 mL of methylene chloride were mixed, and the solution of thiophene-3-carbonyl chloride was added into the flask slowly. After all of the solution was added, the ice bath was removed, and the reactant was stirred at ambient temperature for 30 min. Then, the reactant was washed by water several times, and the organic layer was dried over anhydrous MgSO<sub>4</sub>. After removing solvent, the crude product was purified by flash chromatography (EtOAc/hexane, 1:4) to give 12 g (91%) of compound **5** as pale yellow oil ; <sup>1</sup>H NMR (300 MHz, CDCl<sub>3</sub>): δ 7.46 (d, 1H, *J* = 1.09 Hz), 7.30 (t, 1H, *J* = 1.09 and 4.94 Hz), 7.17 (d, 1H, *J* = 4.94 Hz), 1.18 (m, 10H) ; <sup>13</sup>C NMR (75 MHz, CDCl<sub>3</sub>) δ 166.64, 137.53, 13.08, 125.88, 43.32, 14.59, 39.81 HRMS(EI<sup>+</sup>, *m/z*) [*M*]<sup>+</sup> calcd for C<sub>9</sub>H<sub>13</sub>NOS 183.0718 measured 183.0717

#### II-2-1-4. Synthesis of benzo[1,2-*b*:4,5-*b'*]dithiophene-4,8-dione (6)

Compound **5** (70.93 mol, 12 g) was put into a well-dried flask with 25 mL of THF under an inert atmosphere. The solution was cooled down by an ice-water bath, and 32 mL of *n*-butyllithium (85.12 mol, 2.5 mol/L) was added into the flask dropwise within 30 min. Then, the reactant was stirred at ambient temperature for 2 hr. The reactant was poured into ice water and stirred for several hours. The mixture was filtrated, and the yellow precipitate was washed by 100 mL of water, 50 mL of methanol, and 50 mL of hexane successively. 7.5 g of compound **6** was obtained as a yellow powder (34.04 mmol, yield 96%). Mp 241 °C ; <sup>1</sup>H NMR (300 MHz, CDCl<sub>3</sub>): δ 7.15 (d, 2H, *J* = 4.94 Hz), 6.46 (d, 2H, *J* = 5.22 Hz) ; <sup>13</sup>C NMR (75 MHz, CDCl<sub>3</sub>) δ 174.69, 145.14, 143.06, 133.78, 126.81 HRMS(EI<sup>+</sup>, *m/z*) [*M*]<sup>+</sup> calcd for C<sub>10</sub>H<sub>4</sub>O<sub>2</sub>S<sub>2</sub> 219.9653 measured 219.9652

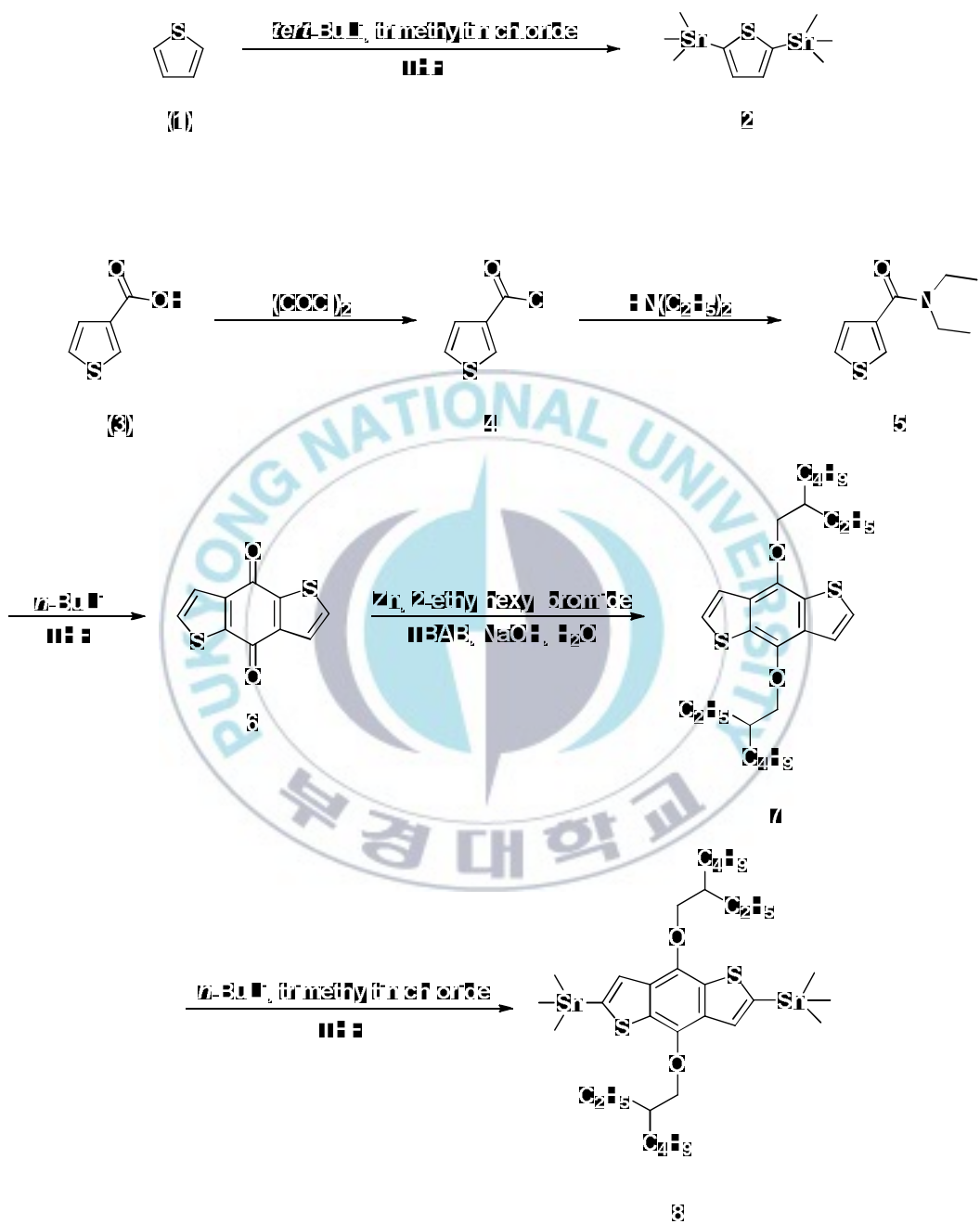
#### II-2-1-5. Synthesis of 4,8-bis(2-ethylhexyloxy)benzo[1,2-*b*:4,5-*b'*]dithiophene (7)

To a mixture of compound **6** (4 g, 18 mmol) and zinc powder (2.6 g, 40 mmol) was added 5*N* NaOH aqueous solution (37 mL) and the mixture was stirred under reflux for 3 hr, After 2-ethylhexyl bromide (22.26 g, 54 mmol) and tetrabutylammoniumbromide (0.9 g, 3.64 mmol) were added to the mixture, the reaction mixture was further refluxed for 12 hr. The reaction mixture was then extracted with diethyl ether, and the organic layer was washed with brine and

dried over anhydrous MgSO<sub>4</sub>. After evaporating the solvent, the crude product was purified by silica gel chromatography using hexane to yield as a light yellow oil, yield 55%. <sup>1</sup>H NMR (CDCl<sub>3</sub>, 400MHz, δ): 7.48(d, 2H, J = 5 Hz), 7.46 (d, 2H, J = 5 Hz), 4.18 (br, 4H), 1.78 (m, 2H), 1.73–1.25 (m, 16H), 0.92–1.03 (t, 12H, J = 7 Hz).

#### II-2-1-6. Synthesis of 2,6-bis(trimethyltin)-4,8-bis(2-ethylhexyloxy)benzo[1,2-*b*:3,4-*b'*]dithiophene (8)

To a solution of compound 7 (4 g, 5.1 mmol) in anhydrous THF (35 mL) was added dropwise *n*-butyllithium (2.5 M in hexane, 8.16 mL, 20.4 mmol) via syringe at -78 °C under nitrogen atmosphere. The mixture was stirred at -78 °C for 30 min and then at room temperature for 30 min. After the mixture was cooled to -78 °C again, trimethyltin chloride (25.5 g, 25.5 mmol) was added. The mixture was warmed to room temperature and stirred for 12 hr. After quenching the reaction with water, the volatile species were evaporated in vacuo. The residue was extracted with hexane, and the organic layer was washed with brine, dried over anhydrous MgSO<sub>4</sub>, and concentrated. The crude product was purified by recrystallization from methanol to yield as a colorless needles (5 g, 4.51 mmol, 88%). M.p. 60-61 °C. <sup>1</sup>H NMR (CDCl<sub>3</sub>, 400MHz, δ): 7.50 (t, 2H, J = 14.64 Hz), 4.17 (d, 4H, J = 5.36 Hz), 1.80 (m, 2H), 1.32-1.72 (m, 16H), 1.01 (t, 6H, J = 7.38 Hz), 0.93 (t, 6H, J = 7.12 Hz), 0.43 (m, 18H)



Scheme 1. Synthetic route of donor monomers.

## II-2-2. Synthesis of acceptor monomers

### II-2-2-1. Synthesis of 2,3-difluoro-1,4-bis-(trimethylsilyl)benzene (10)

*n*-butyllithium (1.6 M in *n*-hexane, 120 mL, 192mmol) was added to a solution of di-isopropylamine (27 mL, 192mmol) in anhydrous THF (80 mL) at -78 °C. After stirring 30 min at -78 °C, 1,2-difluorobenzene (7.5 mL, 77mmol) and chlorotrimethylsilane (24 mL, 192mmol) was added to the solution at a rate which allowed the internal reaction temperature to remain below -50 °C. The solution was stirred at -78 °C for an additional 1 hr. 1 M H<sub>2</sub>SO<sub>4</sub> solution (20 mL) was added and then extracted with diethyl ether (20 mL × 3). The combined organic layers were washed with brine, dried over MgSO<sub>4</sub>, and concentrated under reduced pressure to afford colorless needle-shaped crystals of compound **10** (19.0 g, 98%). <sup>1</sup>H NMR (CDCl<sub>3</sub>, 300MHz, δ): 7.09 (s, 2H), 0.32 (s, 18H). LRMS (EI): m/z = 258 (M<sup>+</sup>).

### II-2-2-2. Synthesis of 1,4-dibromo-2,3-difluoro-benzene (11)

To a neat bromine (5.3 mL, 103mmol) cooled to 0 °C was added portion wise solid **10** (8.9 g, 34.4mmol) while maintaining the internal temperature between 20 and 40 °C. The reaction mixture was stirred at 58 °C for 2 hr. After 1 hr of this period had elapsed, additional bromine (0.9 mL, 17.2mmol) was added. The reaction mixture was cooled to 0 °C and slowly poured into ice-cold saturated

NaHCO<sub>3</sub> solution and extracted with diethyl ether (50 mL × 3). The combined organic layers were washed with brine, dried over MgSO<sub>4</sub>, and concentrated under reduced pressure to afford colorless liquid of compound **11** (9.2 g, 99%).  
<sup>1</sup>H NMR (CDCl<sub>3</sub>, 300MHz, δ): 7.23 (m, 2H). LRMS (EI): m/z = 272 (M<sup>+</sup>).

### II-2-2-3. Synthesis of 1,4-dibromo-2,3-difluoro-5,6-dinitro-benzene (**12**)

In a 500 mL flask, concentrated sulphuric acid (44 mL) was added and cooled to 0-5°C in an ice water bath. Fuming nitric acid (44 mL) and 2,3-difluoro-1,4-dibromo-benzene (8.8 g, 32.5mmol) were slowly added. Then, the flask was heated to 65°C for 14 hr. The mixture was then precipitated into ice water. The resulting yellow solid was filtered and purified by column with petroleum hexane/CH<sub>2</sub>Cl<sub>2</sub> (4:1) to afford a white solid of compound **12** (3.4 g, 29%).

### II-2-2-4. Synthesis of 3,6-dibromo-4,5-difluorobenzene-1,2-diamine (**13**)

To a solution of compound **12** (6.3 g, 17.5mmol) in ethanol (100 mL) and conc. HCl (60mL) was added SnCl<sub>2</sub>•2H<sub>2</sub>O (39.5 g, 175mmol) in several portions. The mixture was refluxed for 1 hr and stirred overnight at room temperature. Then, pH value of the mixture was adjusted to 8~9 by adding aqueous KOH solution. then the mixture was extracted with ethyl acetate three times. The combined organic phases were dried over anhydrous MgSO<sub>4</sub>. Further purification was run by silica column with petroleum hexane/CH<sub>2</sub>Cl<sub>2</sub> (1:1) to give a white-solid of

compound **13** (4.6 g, 88%).  $^1\text{H}$  NMR ( $\text{CDCl}_3$ , 300MHz,  $\delta$ ): 3.85 (s, 4H).  $^{13}\text{C}$  NMR ( $\text{CDCl}_3$ , ppm): 142.99 (d,  $J = 18.11$  Hz), 141.06 (d,  $J = 17.65$  Hz), 129.78, 98.39 (t).  $^{19}\text{F}$  NMR ( $\text{CDCl}_3$ , ppm): -139.02. GC-MS ( $\text{M}^+$ ,  $\text{C}_6\text{H}_4\text{Br}_2\text{F}_2\text{N}_2$ ), calcd, 301.9; found: 302.

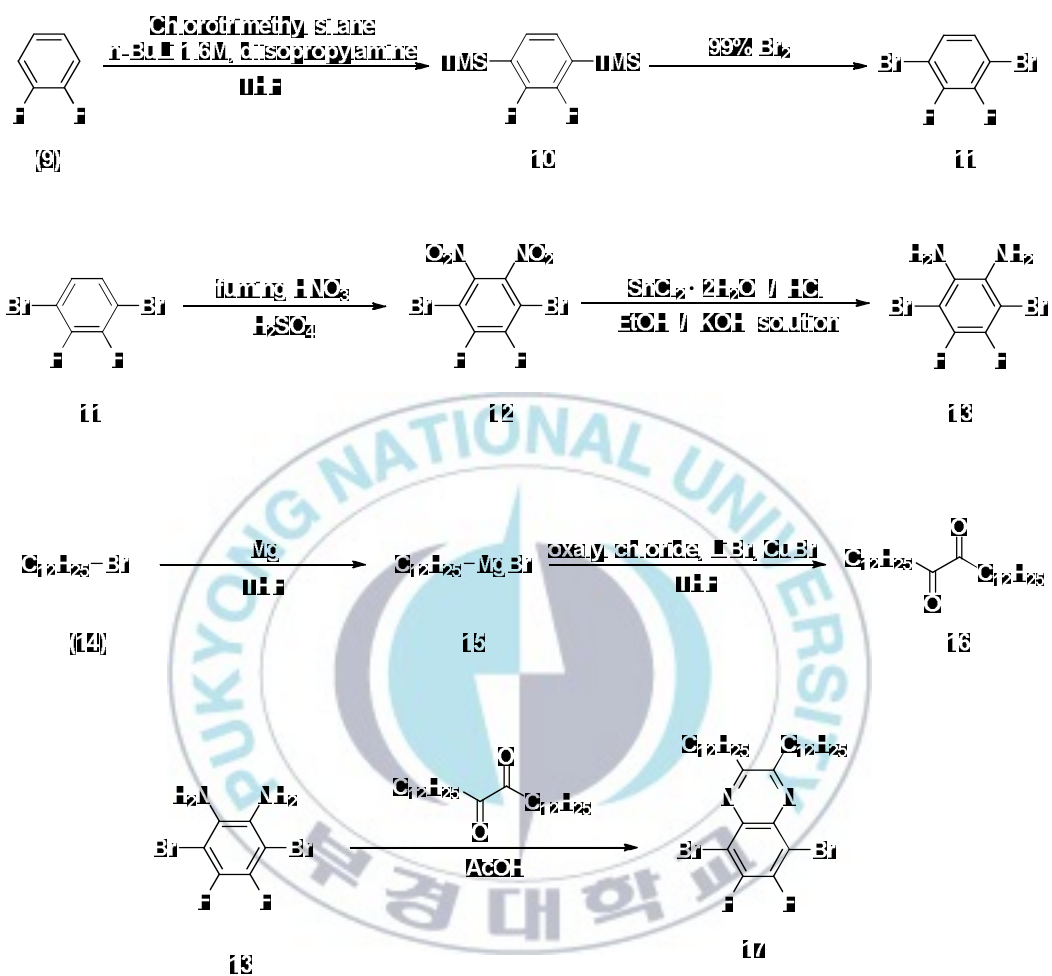
#### II-2-2-5. Synthesis of hexacosane-13,14-dione (**16**)

A Grignard reagent was prepared by the dropwise addition of the respective 1-bromododecane (12.21 ml, 51 mmol) to a stirred suspension of iodine-activated magnesium (1.85 g, 76 mmol) in THF (30 mL). In a separate flask, LiBr (8.05 g, 93 mmol) in THF (150 mL) was added to a stirred suspension of CuBr (7.31 g, 51 mmol) in THF (150 mL) to form a pale green suspension. This mixture was then cooled to  $-78$  °C via a pentane/liquid nitrogen bath. The Grignard reagent was slowly added to the LiBr/CuBr suspension by cannula such that the temperature of the reaction mixture did not exceed  $-75$  °C. Oxalyl chloride (2 ml, 23 mmol) was then added slowly via syringe to maintain a temperature below  $-70$  °C. The mixture was stirred at  $-78$  for 60 min, allowed to warm to room temperature and quenched with saturated aqueous  $\text{NH}_4\text{Cl}$ . The organic layer was separated and the aqueous layer extracted repeatedly with ethyl acetate. The combined organic layers were dried with anhydrous  $\text{Na}_2\text{SO}_4$ , concentrated by rotary evaporation, and separated on a silica column using a 10:1 hexane/methylene chloride mixture. The compound **16** was obtained as a yellow solid (5.36g, 58%).  $^1\text{H}$  NMR ( $\text{CDCl}_3$ ,

400MHz,  $\delta$ ): 2.70 (t, 4H, J = 7.38 Hz), 1.54 (m, 4H, J = 7.12 Hz), 1.23 (m, 36H), 0.85 (t, 6H, J = 6.84 Hz)

#### II-2-2-6. Synthesis of 5,8-dibromo-6,7-difluoro-2,3-didodecylquinoxaline (17)

The compound **13** (2.2 g, 7.3 mmol) and compound **16** (3.48 g, 8.8 mmol) were dissolved in acetic acid (60 mL). The mixture was refluxed overnight. After cooling to room temperature, the resultant mixture was poured into water and extracted with ethylacetate. After dried over MgSO<sub>4</sub> and purified by silica column with petroleum hexane to give a white solid of compound **17** (3.67 g, 66%). <sup>1</sup>H NMR (CDCl<sub>3</sub>, 400MHz,  $\delta$ ): 3.03 (t, 4H, J = 7.66 Hz), 1.88 (m, 4H, J = 7.52 Hz), 1.24-1.44 (m, 36H), 0.86 (t, 6H, J = 6.84 Hz)



Scheme 2. Synthetic route of difluoroquinoxaline (DFQx).

### II-2-2-7. Synthesis of 2,5-dibromo-4-fluoro-nitrobenzene (19)

To a solution of 1,4-dibromo-2-fluorobenzene (5.0 g, 19.7 mmol) in dichloromethane (16 mL), trifluoroacetic acid (8 mL), and trifluoroacetic anhydride (16 mL) at 0 °C was added  $\text{NH}_4\text{NO}_3$  (2 g, 25 mmol), the mixture was then stirred at room temperature overnight. After that, the mixture was poured into water and the aqueous solution was extracted with dichloromethane twice. The combined organic phase was dried over  $\text{MgSO}_4$ . After removing the solvent, the crude compound was purified by silica column to give off white solid (5.0 g, 85%).  $^1\text{H NMR}$  ( $\text{CDCl}_3$ , 300MHz,  $\delta$ ): 8.21 (d,  $J = 6.36$  Hz, 1H), 7.57 (d,  $J = 7.41$  Hz, 1H). GC-MS ( $\text{M}^+$ ,  $\text{C}_6\text{H}_2\text{Br}_2\text{FNO}_2$ ), calcd, 298.9; found: 299.

### II-2-2-8. Synthesis of Synthesis of N-(2',5'-dibromo-4'-fluorophenyl)-2,2,2-trifluoroacetamide (21)

To a solution of compound **19** (5.0 g, 16.7 mmol) in ethanol (16 mL) and conc. HCl (14 mL) at 0 °C was added  $\text{SnCl}_2 \cdot 2\text{H}_2\text{O}$  (20 g, 88 mmol) in several portions. After addition, the mixture was heated to reflux for 45 min and then stirred at room temperature overnight. Aqueous KOH solution was added to adjust the pH value to  $\sim 9$ . Then, the mixture was extracted with dichloromethane three times. The combined organic phases were washed with water twice and dried over anhydrous  $\text{MgSO}_4$ . After removing the solvent, the crude product was dissolved into chloroform (250 mL). The trifluoroacetic anhydride (19 mL) was added into

the mixture slowly and the resulting mixture was stirred at room temperature for 2 hours. The saturated aqueous NaHCO<sub>3</sub> was then added into the mixture, and the organic phase was separated and dried over MgSO<sub>4</sub>. After removing solvent, the crude product was purified by silica column to give a yellow solid (4.1 g, 61%). <sup>1</sup>H NMR (CDCl<sub>3</sub>, 300MHz, δ): 8.62 (d, J = 6.66 Hz, 1H), 8.31 (s, 1H), 7.45 (d, J = 7.32 Hz, 1H). GC-MS(M+, C<sub>8</sub>H<sub>3</sub>Br<sub>2</sub>F<sub>2</sub>NO), caclcd, 364.9; found: 365.

#### **II-2-2-9. Synthesis of N-(2',5'-dibromo-4'-fluoro-6'-nitrophenyl)-2,2,2-trifluoroacetamide(22)**

To a solution of conc. H<sub>2</sub>SO<sub>4</sub> (40 mL) and HNO<sub>3</sub> (20 mL) was added compound **21** (3.8 g, 9.3 mmol) very slowly at -10 °C. The mixture was stirred at this temperature for 2 hours and then poured into ice. The resulting solid was recovered and purified by a short flash column using dichloromethane to give a white solid (3.6 g, 85%). <sup>1</sup>H NMR (CDCl<sub>3</sub>, 300MHz, δ): 7.84 (s, 1H), 7.71 (d, J = 7.11 Hz, 1H).GC-MS(M+, C<sub>8</sub>H<sub>2</sub>Br<sub>2</sub>F<sub>4</sub>N<sub>2</sub>O<sub>3</sub>), caclcd, 409.9; found: 410.

#### **II-2-2-10. Synthesis of 2,5-dibromo-4-fluoro-6-nitroaniline (23)**

In a 100-mL single neck flask, the mixture solution of compound **22** (2 g, 4.9 mmol) in conc. H<sub>2</sub>SO<sub>4</sub> (15 mL) and H<sub>2</sub>O (50 mL) was refluxed for 3 hours. Then, the mixture was slowly added into aqueous KOH, the pH value was then adjusted to ~8-9. The mixture was extracted with ethyl acetate twice. The organic phase

was dried over anhydrous  $\text{MgSO}_4$ . After removing the solvent, the crude product was dried under vacuum and used directly without further purification (1.2 g, 78%).  $^1\text{H}$  NMR ( $\text{CDCl}_3$ , 300MHz,  $\delta$ ): 7.49 (d,  $J = 7.29$  Hz, 1H), 5.05 (s, 2H). GC-MS: ( $\text{M}^+$ ,  $\text{C}_6\text{H}_3\text{Br}_2\text{FN}_2\text{O}_2$ ), caclcd, 313.9; found: 314.

#### II-2-2-11. Synthesis of 2,5-dibromo-4-fluoro-5,6-benzenediamine (24)

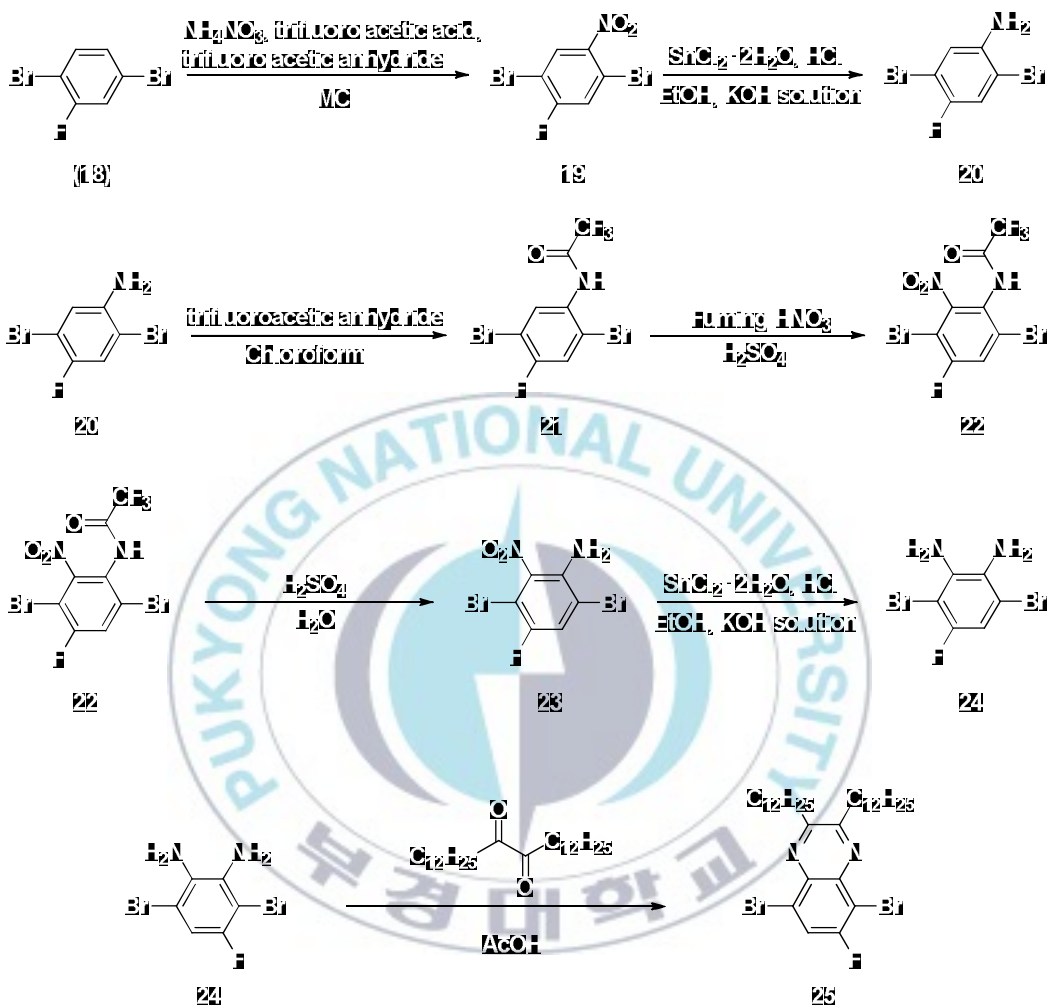
To a solution of compound **23** (1.2 g, 3.8 mmol) in ethanol (15 mL) and conc. HCl (10 mL) was added  $\text{SnCl}_2 \cdot 2\text{H}_2\text{O}$  (6 g, 26 mmol) in several portions. The mixture was refluxed for 1 hour and stirred overnight at room temperature. Then, pH value of the mixture was adjusted to ~8-9 by adding aqueous KOH solution, and then the mixture was extracted with ethyl acetate three times. The combined organic phases were dried over anhydrous  $\text{MgSO}_4$ . Further purification was run by silica column to give an off-white solid (1.0 g, 72%).  $^1\text{H}$  NMR ( $\text{CDCl}_3$ , 300MHz,  $\delta$ ): 6.84 (d,  $J = 8.01$  Hz, 1H), 4.15 (s, 2H), 3.65 (s, 2H).  $^{13}\text{C}$  NMR ( $\text{CDCl}_3$ , 125MHz, ppm): 154.33, 152.41, 135.93 (d,  $J = 3.27$  Hz), 128.92 (d,  $J = 2.59$  Hz), 109.61 (d,  $J = 11.35$  Hz), 109.01 (d,  $J = 26.38$  Hz), 96.95 (d,  $J = 24.14$  Hz). GC-MS ( $\text{M}^+$ ,  $\text{C}_6\text{H}_5\text{Br}_2\text{FN}_2$ ), caclcd, 283.9; found: 284.

#### II-2-2-12. Synthesis of 5,8-dibromo-2,3-didodecyl-6-fluoroquinoxaline (25)

The compound **24** (1.4 g, 4.9 mmol) and compound **16** (2.32 g, 5.9 mmol) were dissolved in acetic acid (60 mL). The mixture was refluxed overnight. After

cooling to room temperature, the resultant mixture was poured into water and extracted with ethylacetate. After dried over  $\text{MgSO}_4$  and purified by silica column with petroleum hexane to give a white solid of compound **25** (2.18 g, 75%).  $^1\text{H}$  NMR ( $\text{CDCl}_3$ , 400MHz,  $\delta$ ): 7.80 (d, 1H,  $J = 8.08$  Hz), 3.04 (m, 4H), 1.88 (m, 4H), 1.24-1.45 (m, 36H), 0.86 (t, 6H,  $J = 6.84$  Hz)





Scheme 3. Synthetic route of monofluoroquinoxaline (FQx).

### II-2-2-13. Synthesis of tributyl(thiophen-2-yl)stannane (26)

To a round bottom flask loaded with dry THF (30 mL), thiophene (5 ml, 63.57 mmol) was added and the mixture was cooled to -78 °C by acetone/dry ice bath. *n*-BuLi in hexane solution (1.6M, 26 mL) was added dropwise. After stirring at -78 °C for 1hr, tributyl tin chloride (12 ml, 42 mmol) was added dropwise and removed the dry ice bath immediately. After six more hours, the reaction was then terminated by adding saturated NaHCO<sub>3</sub> solution (100 ml) into the flask. the solvent was removed by rotary evaporation. The remaining oil was diluted with diethyl ether and washed with brine several times. The collected organic layer was dried over MgSO<sub>4</sub> and the organic solvent was removed by rotary evaporation. The collected orange oil was dried under vacuum for another 3h and used directly for the next step.

### II-2-2-14. Synthesis of 2,3-didodecyl-6,7-difluoro-5,8-di(thiophen-2-yl)quinoxaline (27)

To a solution of compound **17** (2.5 g, 3.8 mmol) and 2-tributylstannylthiophene (4.23 g, 11.4 mmol) in 60 mL *N,N'*-dimethylformamide (DMF) was added Bis(triphenylphosphine)palladium(II) dichloride (PdCl<sub>2</sub>(PPh<sub>3</sub>)<sub>2</sub>) (81 mg, 0.11 mmol) under argon and heated at 85~90 °C for 24 h. Water was then added, and then the mixture was extracted with dichloromethane (CH<sub>2</sub>Cl<sub>2</sub>). The organic phase was washed with water and dried over anhydrous MgSO<sub>4</sub>. The solvent was

removed by rotary evaporation and the residue was recrystallized from ethanol to give compound **27** as a yellow solid (2.04 g, 81%). <sup>1</sup>H NMR (CDCl<sub>3</sub>, 400MHz, δ): 7.98 (d, 2H, J = 2.96 Hz), 7.59 (d, 2H, J = 4.96 Hz), 7.21 (t, 2H, J = 4.56 Hz), 3.06 (t, 4H, J = 7.52 Hz), 1.96 (m, 4H, J = 7.45 Hz), 1.24-1.45 (m, 36H), 0.86 (t, 6H, J = 6.86 Hz)

#### **II-2-2-15. Synthesis of 5,8-bis(5-bromothiophen-2-yl)-2,3-didodecyl-6,7-difluoroquinoxaline (28)**

Compound **27** (2.0 g, 3.0 mmol) was dissolved in THF (60 mL) under nitrogen atmosphere, and NBS (1.1 g, 6.0 mmol) was added. The mixture was stirred at room temperature overnight. After that water (100 mL) was added to quench the reaction, and then extracted with diethyl ether, washed with brine, and dried with anhydrous MgSO<sub>4</sub>. The solvent was removed via rotary evaporation and subsequently purified by recrystallization to afford compound **28** as an orange solid (2.41 g, 95%). <sup>1</sup>H NMR (CDCl<sub>3</sub>, 400MHz, δ): 7.75 (d, 2H, J = 4.00 Hz), 7.14 (d, 2H, J = 4.04 Hz), 3.08 (t, 4H, J = 7.66 Hz), 1.97 (m, 4H, J = 7.46 Hz), 1.23-1.46 (m, 36H), 0.85 (t, 6H, J = 6.84 Hz)

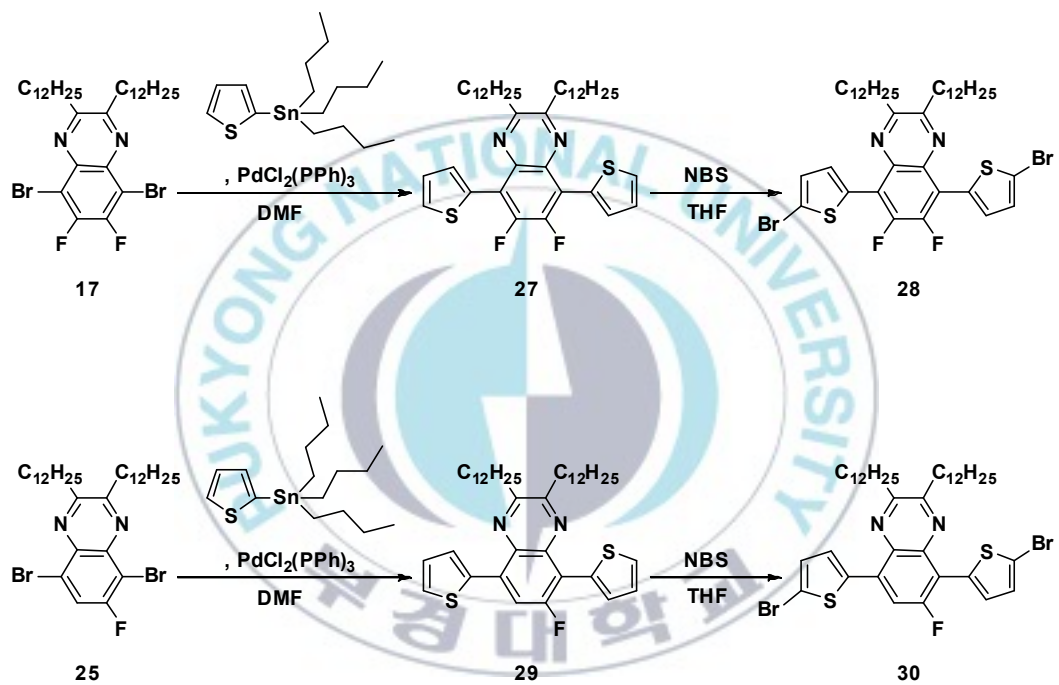
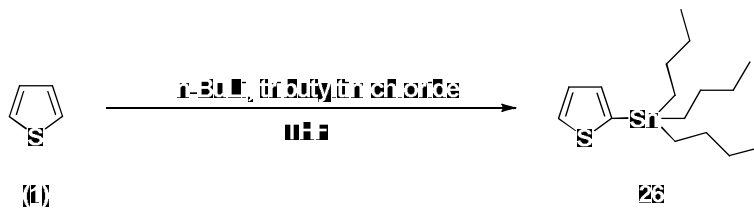
#### **II-2-2-16. Synthesis of 2,3-didodecyl-6-fluoro-5,8-di(thiophen-2-yl)quinoxaline (29)**

To a solution of compound **25** (3.7 g, 5.7 mmol) and 2-tributylstannylthiophene

(6.4 g, 17.2 mmol) in 70 mL *N,N'*-dimethylformamide (DMF) was added Bis(triphenylphosphine)palladium(II) dichloride ( $\text{PdCl}_2(\text{PPh}_3)_2$ ) (120 mg, 0.17 mmol) under argon and heated at 85~90 °C for 24 h. Water was then added, and then the mixture was extracted with dichloromethane ( $\text{CH}_2\text{Cl}_2$ ). The organic phase was washed with water and dried over anhydrous  $\text{MgSO}_4$ . The solvent was removed by rotary evaporation and the residue was recrystallized from ethanol to give compound **29** as a yellow solid (2.78 g, 75%).  $^1\text{H}$  NMR ( $\text{CDCl}_3$ , 400MHz,  $\delta$ ): 7.82 (m, 3H), 7.5 (m, 2H), 7.19 (m, 2H), 3.04 (m, 4H), 1.97 (m, 4H), 1.24-1.45 (m, 36H), 0.86 (t, 6H,  $J = 6.86$  Hz)

#### II-2-2-17. Synthesis of 5,8-bis(5-bromothiophen-2-yl)-2,3-didodecyl-6-fluoroquinoxaline (**30**)

Compound **29** (2.5 g, 3.85 mmol) was dissolved in THF (60 mL) under nitrogen atmosphere, and NBS (1.2 g, 7.7 mmol) was added. The mixture was stirred at room temperature overnight. After that water (100 mL) was added to quench the reaction, and then extracted with diethyl ether, washed with brine, and dried with anhydrous  $\text{MgSO}_4$ . The solvent was removed via rotary evaporation and subsequently purified by recrystallization to afford compound **30** as an orange solid (2.87 g, 92%).  $^1\text{H}$  NMR ( $\text{CDCl}_3$ , 400MHz,  $\delta$ ): 7.80 (d, 1H,  $J = 13.72$  Hz), 7.72 (m, 1H), 7.49 (d, 1H,  $J = 4.04$  Hz), 7.10 (m, 2H,  $J = 4.03$ ), 3.07 (m, 4H), 1.98 (m, 4H), 1.24-1.44 (m, 36H), 0.86 (t, 6H,  $J = 6.72$  Hz)

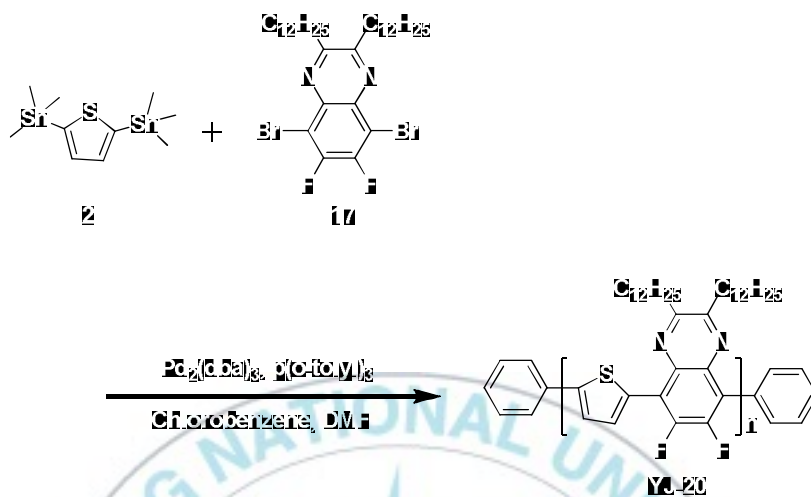


**Scheme 4.** Synthetic route of di(thiophenyl)quinoxalines (DTDFQx, DTFQx).

## II-3. Synthesis of polymer

### II-3-1. Synthesis of poly[2,3-didodecyl-6,7-difluoro-5-(thiophen-2-yl)quinoxaline] (YJ-20)

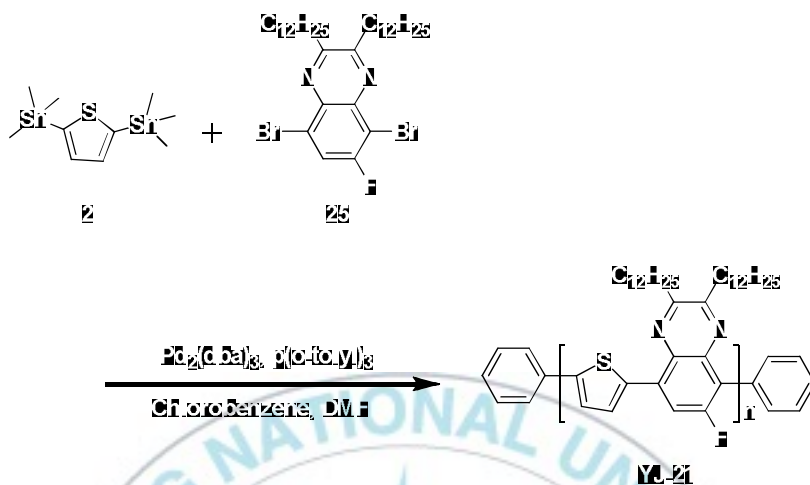
In a 25 mL dry flask, 5,8-dibromo-2,3-didodecyl-6,7-difluoroquinoxaline (**17**) (0.3303 g, 0.5 mmol) and 2,5-bis(trimethylstannyl)thiophene (**2**) (0.2112 g, 0.5 mmol) were dissolved in a mixture of degassed chlorobenzene (6 mL) and *N,N*-dimethylformamide (1 mL), under argon atmosphere. tris(dibenzylideneacetone) dipalladium (0) ( $\text{Pd}_2(\text{dba})_3$ ) (23 mg, 0.025 mmol) and  $\text{P}(o\text{-tolyl})_3$  (61 mg, 0.2 mmol) were added. Then the mixture was vigorously stirred at 100~110 °C for 48~72 hr. After cooling down, the solution was poured into methanol. The polymer was collected by filtration and was Soxhlet-extracted in order with methanol, hexane, and then with chloroform. The chloroform solution was concentrated to a small volume, and the polymer was precipitated by pouring this solution into methanol. Finally, the polymer was collected by filtration, dried under vacuum at 50 °C overnight and afforded PTDFQx (259 mg) in yield 88%.



Scheme 5. Synthetic route of PTDFQx (YJ-20).

### II-3-2. Synthesis of poly[2,3-didodecyl-7-fluoro-5-(thiophen-2-yl)quinoxaline] (YJ-21)

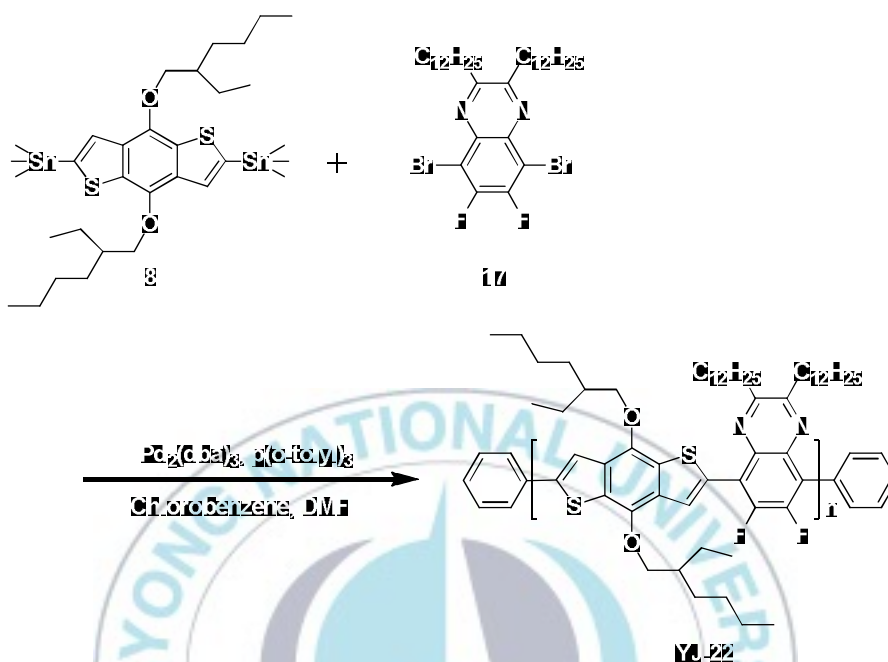
In a 25 mL dry flask, 5,8-dibromo-2,3-didodecyl-6-fluoroquinoxaline (**25**) (0.3213 g, 0.5 mmol) and 2,5-bis(trimethylstannyl)thiophene (**2**) (0.2112 g, 0.5 mmol) were dissolved in a mixture of degassed chlorobenzene (6 mL) and *N,N'*-dimethylformamide (1 mL). under argon atmosphere. tris(dibenzylideneacetone) dipalladium (0) ( $\text{Pd}_2(\text{dba})_3$ ) (23 mg, 0.025 mmol) and  $\text{P}(o\text{-tolyl})_3$  (61 mg, 0.2 mmol) were added. Then the mixture was vigorously stirred at 100~110 °C for 48~72 hr. After cooling down, the solution was poured into methanol. The polymer was collected by filtration and was Soxhlet-extracted in order with methanol, hexane, chloroform and then with toluene. The toluene solution was concentrated to a small volume, and the polymer was precipitated by pouring this solution into methanol. Finally, the polymer was collected by filtration, dried under vacuum at 50 °C overnight and afforded PTFQx (258 mg) in yield 91%.



Scheme 6. Synthetic route of PTFQx (YJ-21).

### II-3-3. Synthesis of poly[5-(4,8-bis((2-ethylhexyl)oxy)benzo[1,2-b:4,5-b']dithiophen-2-yl)-2,3-didodecyl-6,7-difluoroquinoxaline] (YJ-22)

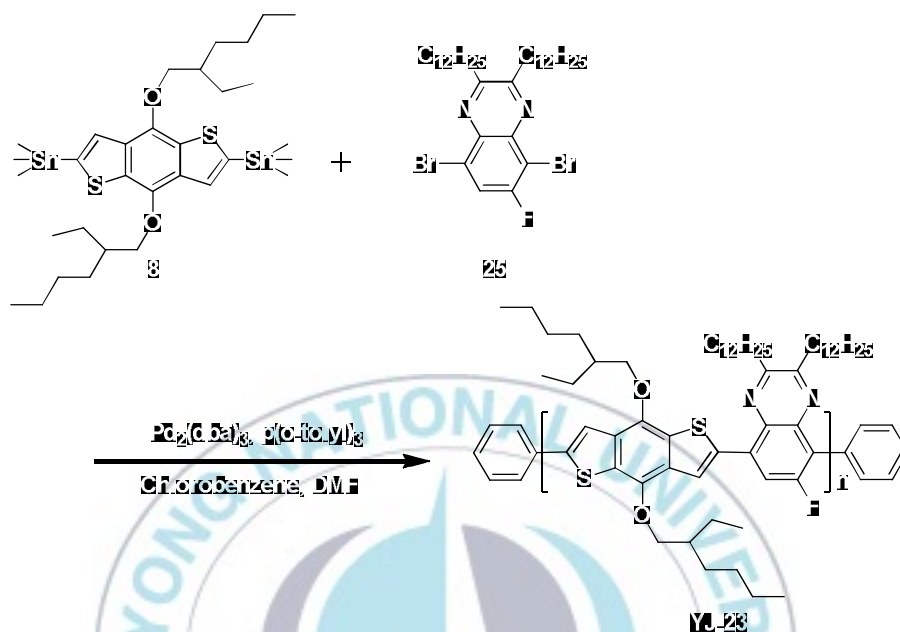
In a 25 mL dry flask, 5,8-dibromo-2,3-didodecyl-6,7-difluoroquinoxaline (**17**) (0.5406 g, 0.7 mmol) and (4,8-bis((2-ethylhexyl)oxy)benzo[1,2-b:4,5-b']dithiophene-2,6-diyl)bis(trimethylstannane) (**8**) (0.4624 g, 0.7 mmol) were dissolved in a mixture of degassed chlorobenzene (8 mL) and *N,N*-dimethylformamide (2 mL). under argon atmosphere. tris(dibenzylideneacetone) dipalladium (0) ( $\text{Pd}_2(\text{dba})_3$ ) (32 mg, 0.035 mmol) and  $\text{P}(o\text{-tolyl})_3$  (85 mg, 0.28 mmol) were added. Then the mixture was vigorously stirred at 100~110 °C for 48~72 hr. After cooling down, the solution was poured into methanol. The polymer was collected by filtration and was Soxhlet-extracted in order with methanol, hexane, and then with chloroform. The chloroform solution was concentrated to a small volume, and the polymer was precipitated by pouring this solution into methanol. Finally, the polymer was collected by filtration, dried under vacuum at 50 °C overnight and afforded PBDTDFQx (112 mg) in yield 24%.



Scheme 7. Synthetic route of PBDTDFQ<sub>x</sub> (YJ-22).

#### II-3-4. Synthesis of poly[5-(4,8-bis((2-ethylhexyl)oxy)benzo[1,2-b:4,5-b']dithiophen-2-yl)-2,3-didodecyl-7-fluoroquinoxaline] (YJ-23)

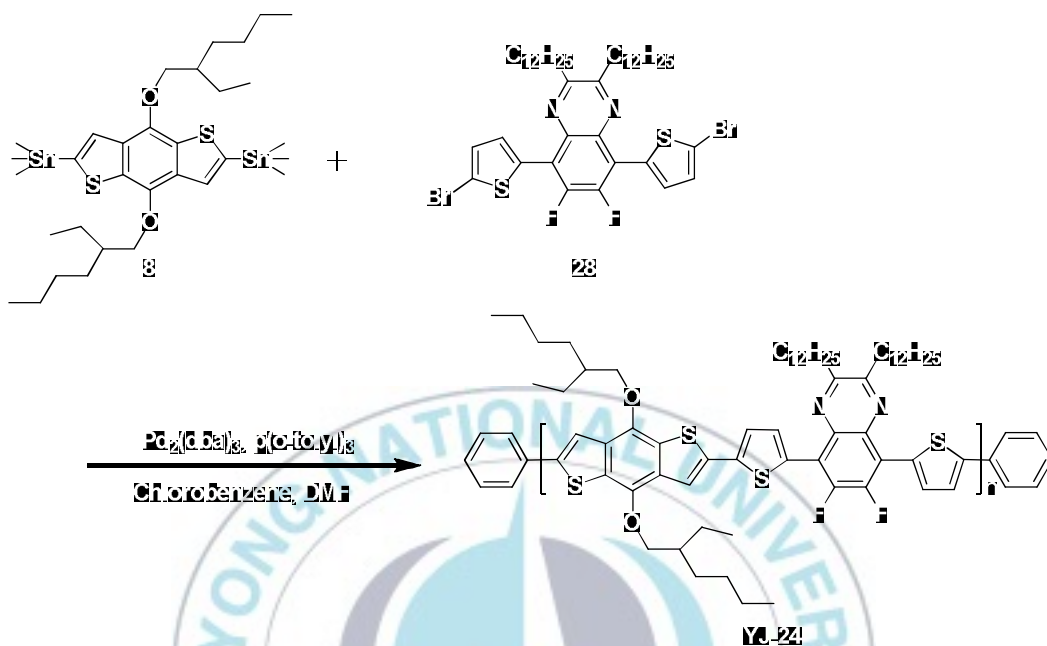
In a 25 mL dry flask, 5,8-dibromo-2,3-didodecyl-6-fluoroquinoxaline (**25**) (0.3213 g, 0.5 mmol) and (4,8-bis((2-ethylhexyl)oxy)benzo[1,2-b:4,5-b']dithiophene-2,6-diyl)bis(trimethylstannane) (**8**) (0.3862 g, 0.5 mmol) were dissolved in a mixture of degassed chlorobenzene (7 mL) and *N,N*-dimethylformamide (2 mL). under argon atmosphere. tris(dibenzylideneacetone) dipalladium (0) (Pd<sub>2</sub>(dba)<sub>3</sub>) (23 mg, 0.025 mmol) and P(*o*-tolyl)<sub>3</sub> (61 mg, 0.2 mmol) were added. Then the mixture was vigorously stirred at 100~110 °C for 48~72 hr. After cooling down, the solution was poured into methanol. The polymer was collected by filtration and was Soxhlet-extracted in order with methanol, hexane and then with chloroform. The chloroform solution was concentrated to a small volume, and the polymer was precipitated by pouring this solution into methanol. Finally, the polymer was collected by filtration, dried under vacuum at 50 °C overnight and afforded PBDTFQx (291 mg) in yield 63%.



Scheme 8. Synthetic route of PBDTFQ<sub>x</sub> (YJ-23).

### II-3-5. Synthesis of poly[5-(5-(4,8-bis((2-ethylhexyl)oxy)benzo[1,2-b:4,5-b']dithiophen-2-yl)thiophen-2-yl)-2,3-didodecyl-6,7-difluoro-8-(thiophen-2-yl)quinoxaline] (YJ-24)

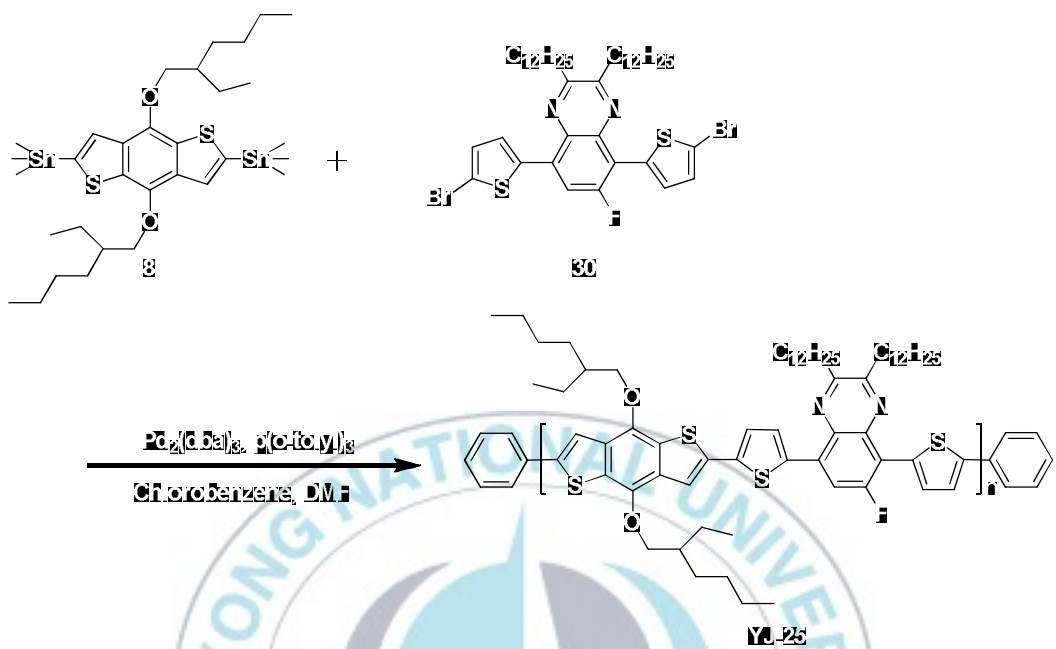
In a 50 mL dry flask, 5,8-bis(5-bromothiophen-2-yl)-2,3-didodecyl-6,7-difluoroquinoxaline (**28**) (0.5774 g, 0.7 mmol) and (4,8-bis((2-ethylhexyl)oxy)benzo[1,2-b:4,5-b']dithiophene-2,6-diyl)bis(trimethylstannane) (**8**) (0.5406 g, 0.7 mmol) were dissolved in a mixture of degassed chlorobenzene (8 mL) and *N,N'*-dimethylformamide (2 mL) under argon atmosphere. tris(dibenzylideneacetone) dipalladium (0) ( $\text{Pd}_2(\text{dba})_3$ ) (32 mg, 0.035 mmol) and  $\text{P}(o\text{-tolyl})_3$  (85 mg, 0.28 mmol) were added. Then the mixture was vigorously stirred at 100~110 °C for 48~72 hr. After cooling down, the solution was poured into methanol. The polymer was collected by filtration and was Soxhlet-extracted in order with methanol, hexane and then with chloroform. The chloroform solution was concentrated to a small volume, and the polymer was precipitated by pouring this solution into methanol. Finally, the polymer was collected by filtration, dried under vacuum at 50 °C overnight and afforded PBDTDTDFQx (775 mg) in yield 99%.



Scheme 9. Synthetic route of PBDTDTDFQ<sub>x</sub> (YJ-24).

### II-3-6. Synthesis of poly[8-(5-(4,8-bis((2-ethylhexyl)oxy)benzo[1,2-b:4,5-b']dithiophen-2-yl)thiophen-2-yl)-2,3-didodecyl-6-fluoro-5-(thiophen-2-yl)quinoxaline] (YJ-25)

In a 50 mL dry flask, 5,8-bis(5-bromothiophen-2-yl)-2,3-didodecyl-6-fluoroquinoxaline (**30**) (0.5648 g, 0.7 mmol) and (4,8-bis((2-ethylhexyl)oxy)benzo[1,2-b:4,5-b']dithiophene-2,6-diyl)bis(trimethylstannane) (**8**) (0.5406 g, 0.7 mmol) were dissolved in a mixture of degassed chlorobenzene (8 mL) and *N,N'*-dimethylformamide (2 mL) under argon atmosphere. tris(dibenzylideneacetone) dipalladium (0) ( $\text{Pd}_2(\text{dba})_3$ ) (32 mg, 0.035 mmol) and  $\text{P}(o\text{-tolyl})_3$  (85 mg, 0.28 mmol) were added. Then the mixture was vigorously stirred at 100~110 °C for 48~72 hr. After cooling down, the solution was poured into methanol. The polymer was collected by filtration and was Soxhlet-extracted in order with methanol, hexane and then with chloroform. The chloroform solution was concentrated to a small volume, and the polymer was precipitated by pouring this solution into methanol. Finally, the polymer was collected by filtration, dried under vacuum at 50 °C overnight and afforded PBDTDTFQ<sub>x</sub> (759 mg) in yield 99%.



Scheme 10. Synthetic route of PBDTDTFQx (YJ-25).

## Chapter III. Results and Discussion

### III-1. Polymerization Results

The solubility is different among these polymers. YJ-20, YJ-22, YJ-23, YJ-24 and YJ-25 can dissolve completely in chloroform, toluene and 1,2-dichlorobenzene (o-DCB) at elevated temperature, YJ-21 can dissolve partially in chloroform, but completely dissolve in the other solvents at elevated temperature.

Molecular weight of the polymers and polydispersity (PDI) was measured by gel permeation chromatography (GPC) method using polystyrene as standard and toluene as eluent (Table III-1). Although YJ-21, YJ-24, YJ-25 showed poor solubility in toluene at room temperature and could not be analyzed, the other three polymers were soluble in toluene which is used as the eluent in the GPC system.

**Table III-1.** Polymerization results.

polymers	YJ - 20	YJ - 21	YJ - 22	YJ - 23	YJ - 24	YJ - 25
$M_n^a$	15667	-	34378	65938	-	-
$M_w^a$	19210	-	59038	99824	-	-
PDI <sup>a</sup>	1.23	-	1.72	1.47	-	-

<sup>a</sup>Number-average molecular weight ( $M_n$ ), weight-average molecular weight ( $M_w$ ) and polydispersity of the polymers were determined by gel permeation chromatography (GPC) in toluene using polystyrene standards.

The thermal properties were analyzed by TGA methods (Figures III-1, Table III-2). TGA revealed that all polymers possess similar thermal stability with a 5% weight loss temperature ( $T_d$ ) over 300 °C. The polymers were showed somewhat low thermal stability, but similar to that reported for alternating copolymers with almost identical constitution units.

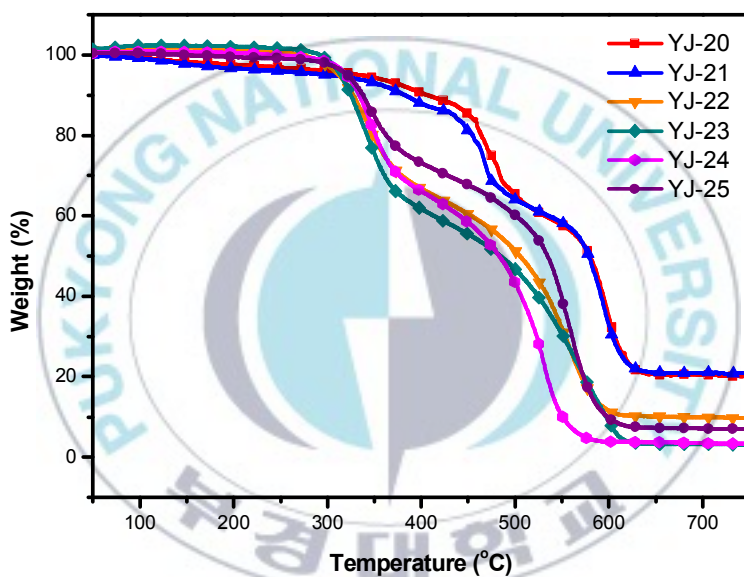


**Figure III-1.** Thermo gravimetric analysis of polymers.

**Table III-2.** Decomposition temperatures of polymers.

polymers	YJ - 20	YJ - 21	YJ - 22	YJ - 23	YJ - 24	YJ - 25
$T_d$ (°C)	334.78	300.76	311.75	313.77	320.41	321.19

Onset decomposition temperatures ( $T_d$ ) (5% weight loss) measured by TGA under Air

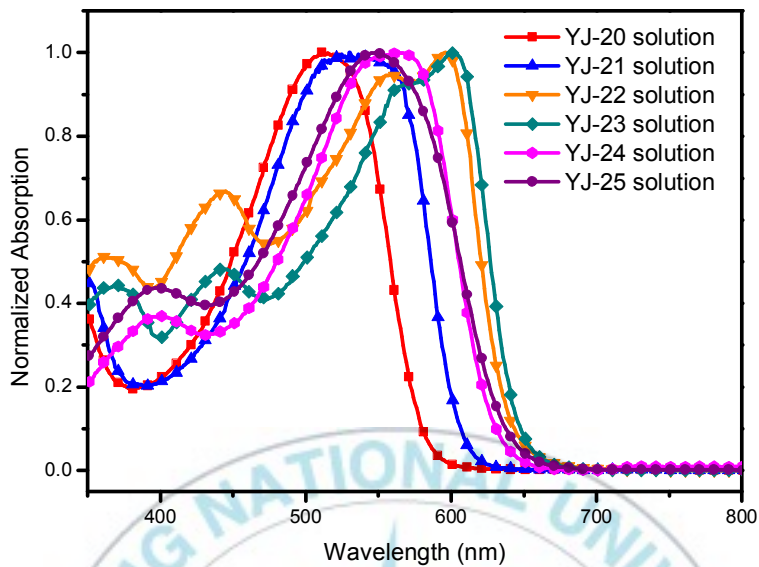
## III-2. Optical Properties of Polymers

Figure III-2 and Figure III-3 shows the absorption spectra of polymers in o-DCB solution and in solid thin film, respectively. The absorption bands in the film have maximum peaks at 572~609 nm, and are red-shifted than those in solution where two peaks are found to be 512~602 nm. The bathochromic shift in the solid state indicates an increased  $\pi$ - $\pi$  stacking form and stronger electronic interaction between the individual polymer chains in the solid state, which is related to its semi-crystalline structure. The optical bandgap ( $E_g^{\text{opt}}$ ) deduced from the onset (637~660 nm) of the polymer absorption spectrum in the films is 1.88~1.95 eV, which are known as the medium bandgap of a donor polymer in field of BHJ solar cells.

**Table III-3.** Optical properties of polymers.

polymer	Abs.			$E_g^{\text{opt}}$ (eV)
	solution <sup>a</sup> $\lambda_{\text{max}}$ (nm)	film $\lambda_{\text{max}}$ (nm)	film $\lambda_{\text{edge}}$ (nm)	
YJ - 20	512	593	637	1.95
YJ - 21	530	609	652	1.90
YJ - 22	596	601	652	1.90
YJ - 23	602	606	654	1.89
YJ - 24	568	578	651	1.90
YJ - 25	548	572	660	1.88

<sup>a</sup> In o-DCB solution.



**Figure III-2.** UV-visible absorption spectra of polymers in o-dichlorobenzene solution.

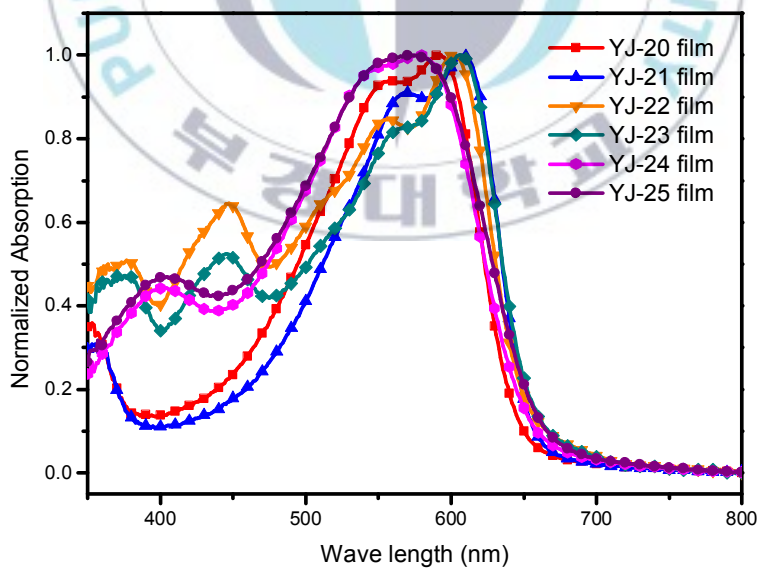


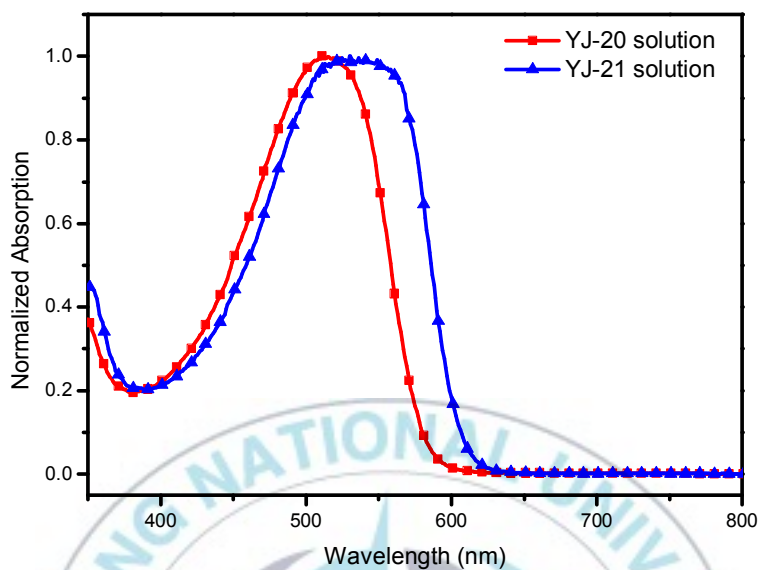
**Figure III-3.** UV-visible absorption spectra of polymers in a thin film formed via spin-cast from a solution in o-dichlorobenzene (1wt%).

As shown in Figure III-4 and Figure III-5, absorption spectra of YJ-20 and YJ-21 in film state obtain the great value of bathochromic shift (about 80 nm at maximum peak) compared to solution state. These confirmed that two polymers have significantly fine intermolecular interaction and enhanced  $\pi$ - $\pi$  stacking in solid state, due to existence of low steric hindrance in repeating units.

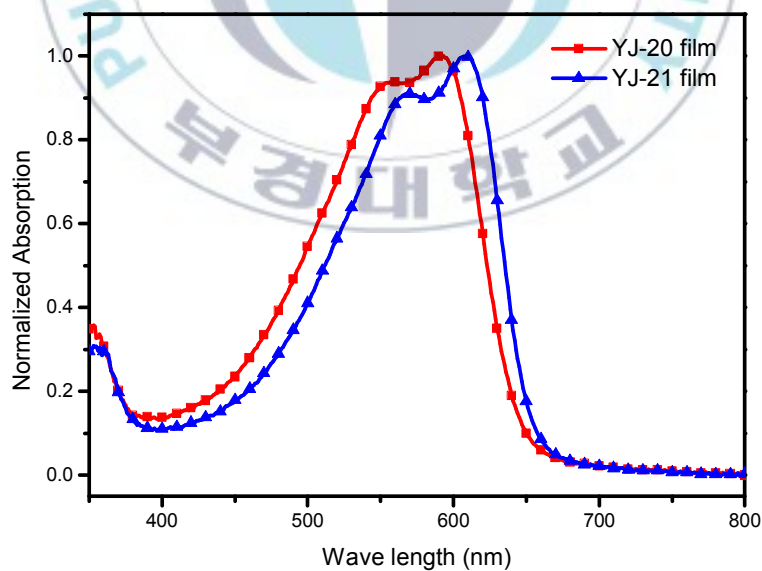
The absorption spectra of YJ-22 and YJ-23 were displayed in Figure III-6 and Figure III-7. These two polymers had similar spectra in both film state and solution state. The value bathochromic shift was about 5 nm at maximum peaks in film state.

Figure III-8 and figure III-9 showed absorption spectra of YJ-24 and YJ-25. In solution state, the maximum peak of YJ-24 and YJ-25 spectra be found at 568, 548 nm and the bathochromic shift in each film states was about 10, 24 nm respectively. Although the smaller amount of shift was showed than that of YJ-20 and YJ-21, the absorption spectra of this series in film states obtained a much broader peaks.

The polymers containing monofluorinated quinoxaline (YJ-21, 23, 25) displayed narrow optical band gaps compared with difluorinated quinoxaline polymers (YJ-20, 22, 24). This can be partly attributed to a change in the polymer chain packing via the additional non-covalent interactions with a greater number of F atoms.<sup>64</sup>



**Figure III-4.** UV-visible absorption spectra of YJ-20(red) and YJ-21(blue) in o-dichlorobenzene solution.



**Figure III-5.** UV-visible absorption spectra of YJ-20(red) and YJ-21(blue) in a thin film formed via spin-cast from a solution in o-dichlorobenzene (1wt%).

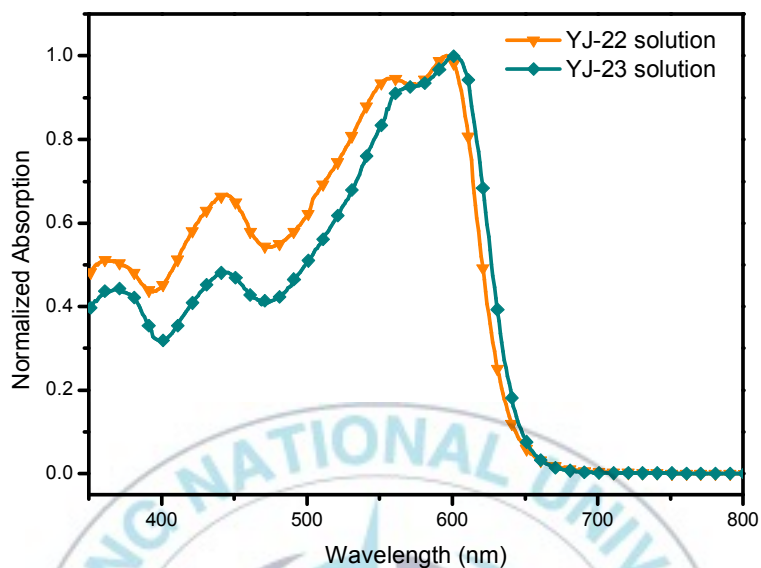


**Figure III-6.** UV-visible absorption spectra of YJ-22(orange) and YJ-23(green) in o-dichlorobenzene solution.

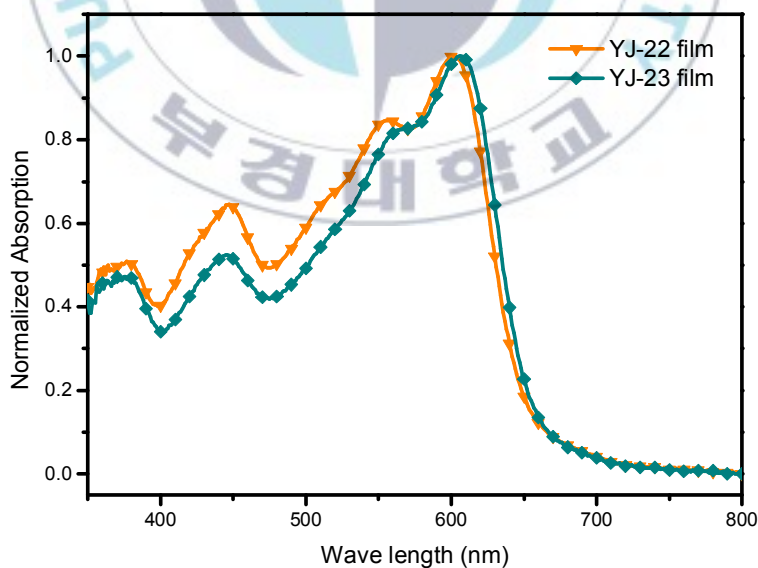


**Figure III-7.** UV-visible absorption spectra of YJ-22(orange) and YJ-23(green) in a thin film formed via spin-cast from a solution in o-dichlorobenzene (1wt%).

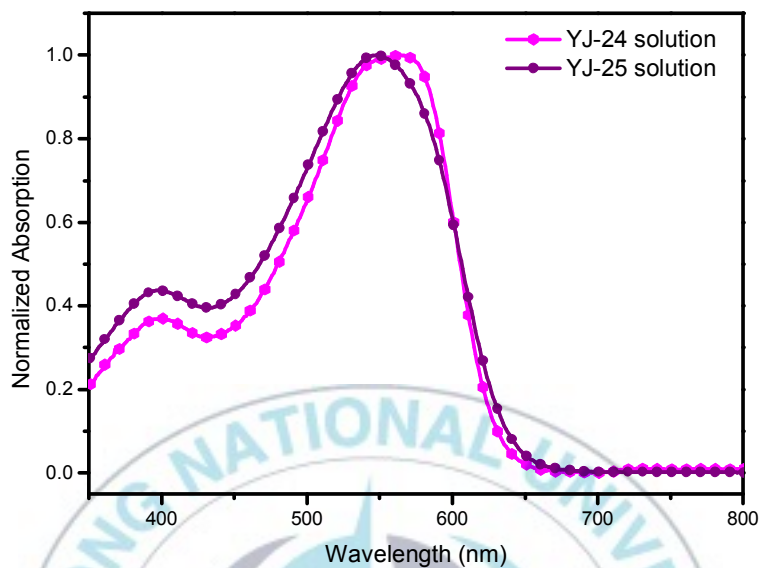


**Figure III-8.** UV-visible absorption spectra of YJ-24(pink) and YJ-25(purple) in o-dichlorobenzene solution.

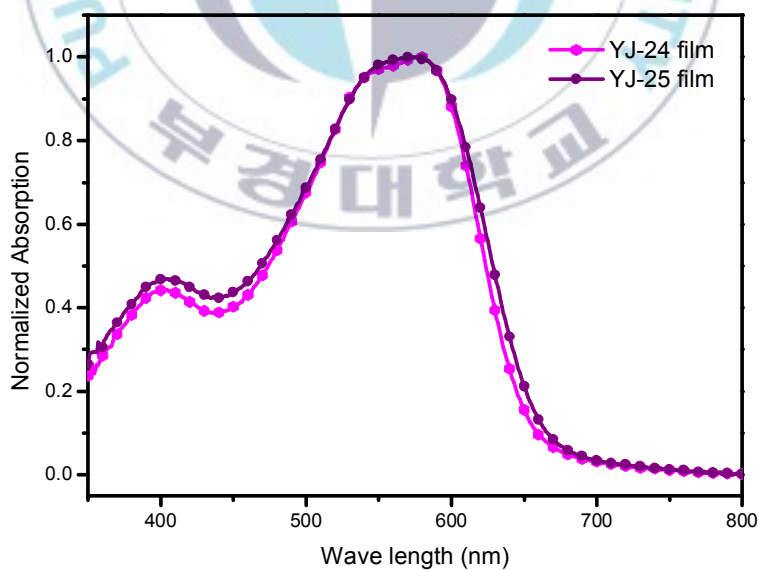


**Figure III-9.** UV-visible absorption spectra of YJ-24(pink) and YJ-25(purple) in a thin film formed via spin-cast from a solution in o-dichlorobenzene (1wt%).

### III-3. Electrochemical Properties of Polymers

The HOMO and LUMO energy levels of these polymers were investigated by cyclic voltammetry (Figure III-10). The onset oxidation potential ( $E_{\text{onset}}^{\text{ox}}$ )/onset reduction potential ( $E_{\text{onset}}^{\text{red}}$ ) of YJ-20 ~ 25 were 0.89/-1.31, 0.81/-1.23, 0.86/-1.40, 0.72/-1.36, 0.74/-1.26 and 0.59/-1.38 V vs Ag/Ag<sup>+</sup>, respectively. From the values of  $E_{\text{onset}}^{\text{ox}}$  and  $E_{\text{onset}}^{\text{red}}$  of the polymers, the HOMO and the LUMO values as well as the electrochemical band gaps ( $E_g^{\text{cv}}$ ) were calculated and also listed in Table III-4 and Figure III-10. The HOMO energy levels of polymers(YJ-20, YJ-22, YJ-24), containing difluorinated quinoxaline unit (DFQx), are lower than identical backboned polymers(YJ-21, YJ-23, YJ-25), containing monofluorinated quinoxaline (FQx), respectively. As well-known, it was verified that inserting fluorine atoms can lower the HOMO level of polymer. The LUMO energy levels of the polymers (-3.57~-3.40 eV) are all similar to a suitable range (less than -3.4) and are slightly higher-lying than that of PCBM (ca. -3.70 eV); thus, efficient charge transfer (exciton dissociation) could be expected to occur in their corresponding devices.

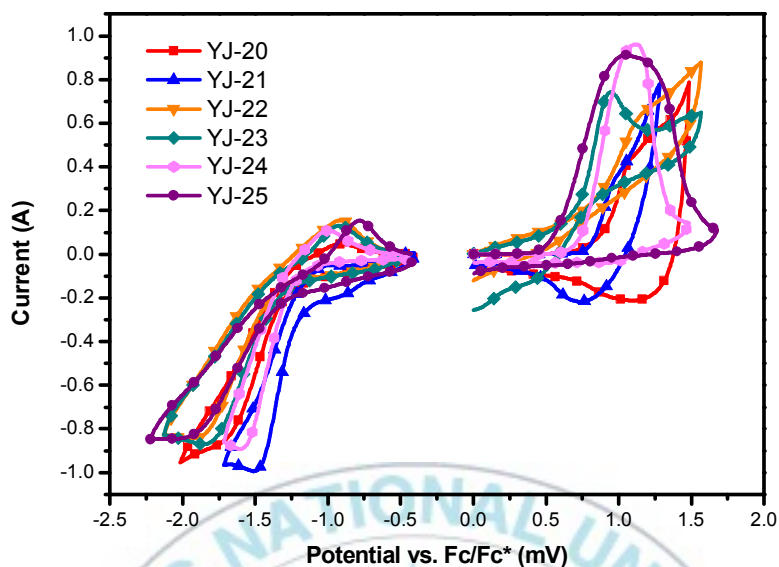


**Figure III-10.** Cyclic voltammety curves of the polymers in 0.1 M  $\text{Bu}_4\text{NPF}_6$  acetonitrile solution at a scan rate of 100 mV/s at room temperature (vs an Ag quasi-reference electrode).

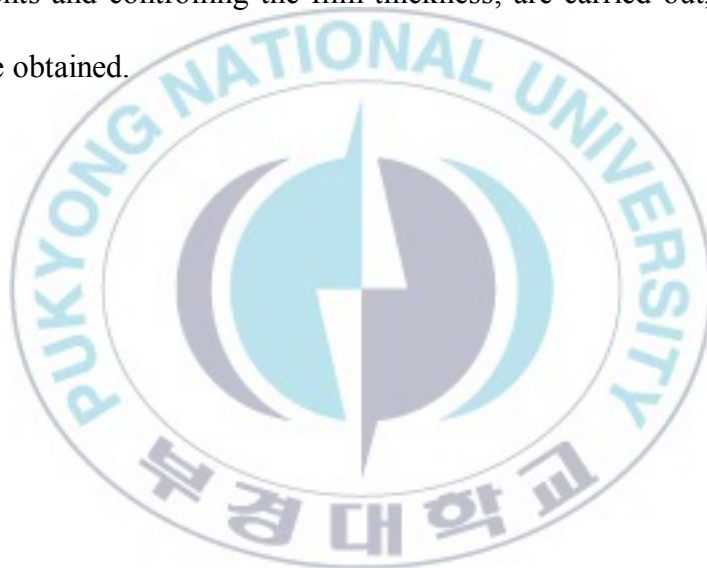
**Table III-4.** Electrochemical Properties of the Polymers.

Polymer	CV		
	HOMO (eV)	LUMO (eV)	$E_g^{\text{cv}}$ (eV)
YJ-20	-5.69	-3.49	2.20
YJ-21	-5.61	-3.57	2.04
YJ-22	-5.66	-3.40	2.26
YJ-23	-5.52	-3.44	2.08
YJ-24	-5.54	-3.54	2.00
YJ-25	-5.39	-3.42	1.97

### III-4. Photovoltaic Properties of Polymers

In order to investigate the photovoltaic properties of the polymers, the polymer solar cells were fabricated with a general device structure of ITO/PEDOT:PSS/polymer:PCBM/Al. At first, the photoactive layer was composed of D/A blend with different ratio (1:0.5, 1:1, 1:2, 1:3) without any post process and solvent additives due to find the optimum ratio. The best performance of devices based on YJ-20~YJ-25 was showed in blend ratio of 1:0.5 (YJ-20), 1:1 (YJ-21), 1:3 (YJ-22), 1:2 (YJ-23), 1:2 (YJ-24) and 1:3 (YJ-25), respectively. As mentioned in section of optical properties, it seemed that the excessive alkyl groups lead to interrupt of not only forming  $\pi$ - $\pi$  stacking but also docking of acceptor on polymer backbones because PCEs of devices based on YJ-22, 23 scarcely improved when ratio of polymer exceeded that of acceptor or otherwise. YJ-20, 21 required a relatively small ratio in order to enhance the performance of these devices. YJ-20, 21 was observed PCE of 1.95 with 1:0.5 ratio and 2.02 with 1:1 ratio, respectively. The device of YJ-24:PCBM with 1:2 ratio had the best performance among the all devices, obtained PCE of 3.12 %. Compared with YJ-22, YJ-24 includes a thiophene bridge playing a role as molecular spacer on conjugated backbone. It provides enough spaces that the extremely bulky alkyl groups are able to exist on. As a result, that facilitates minimized steric hindrance, forming favorable  $\pi$ - $\pi$  stacking and docking of acceptor on polymer backbones.

We had anticipated that YJ-25-based device also displayed good photovoltaic performance, because YJ-25 had the same backbone even if functional group was different. However, YJ-25 required the more ratio of acceptor and made a poorer efficiency (0.76 %). In the quest to improve the PCEs, the YJ-24:PC<sub>70</sub>BM (1:1.5) device processed with 3 vol % DIO solvent additive exhibits an increase in the PCE of up to 4.75 %. When the additional processes, such as thermal annealing, post treatments and controlling the film thickness, are carried out, the improved PCEs can be obtained.



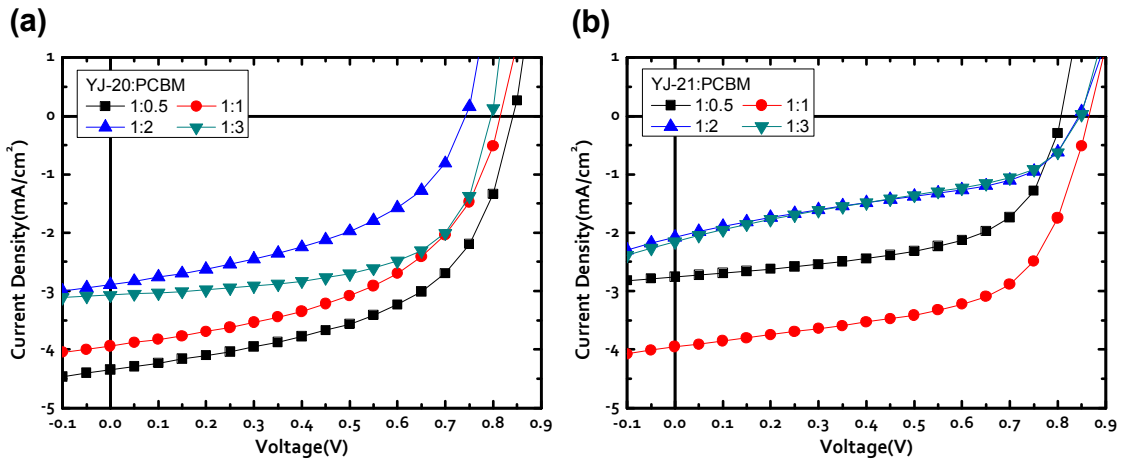


**Figure III-11.** (a) J-V characteristics of the device based on YJ-20:PCBM blend and (b) YJ-21:PCBM blend.

**Table III-5.** Photovoltaic performance of devices based on YJ-20 or YJ-21.

polymer	ratio (polymer:PCBM)	$J_{sc}$ ( $\text{mA}/\text{cm}^2$ )	$V_{oc}$ (V)	FF	PCE (%)
YJ-20	1 : 0.5	4.35	0.85	0.53	1.95
	1 : 1	3.94	0.81	0.50	1.62
	1 : 2	2.89	0.75	0.46	0.99
	1 : 3	3.07	0.80	0.61	1.50
YJ-21	1 : 0.5	2.76	0.81	0.58	1.28
	1 : 1	3.95	0.87	0.59	2.02
	1 : 2	2.08	0.85	0.44	0.78
	1 : 3	2.15	0.85	0.41	0.75

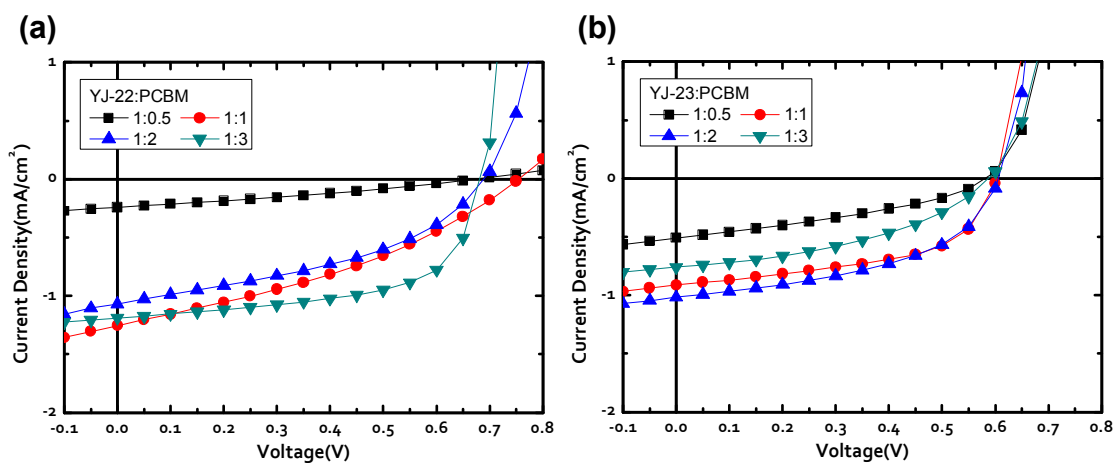


**Figure III-12.** (a) J-V characteristics of the device based on YJ-22:PCBM blend and (b) YJ-23:PCBM blend.

**Table III-6.** Photovoltaic performance of devices based on YJ-22 or YJ-23.

polymer	ratio (polymer:PCBM)	$J_{sc}$ (mA/cm <sup>2</sup> )	$V_{oc}$ (V)	FF	PCE (%)
YJ-22	1 : 0.5	0.24	0.67	0.30	0.05
	1 : 1	1.26	0.75	0.35	0.33
	1 : 2	1.07	0.69	0.41	0.30
	1 : 3	1.19	0.69	0.59	0.49
YJ-23	1 : 0.5	0.51	0.59	0.35	0.11
	1 : 1	0.91	0.60	0.53	0.29
	1 : 2	1.02	0.61	0.48	0.30
	1 : 3	0.76	0.59	0.42	0.19

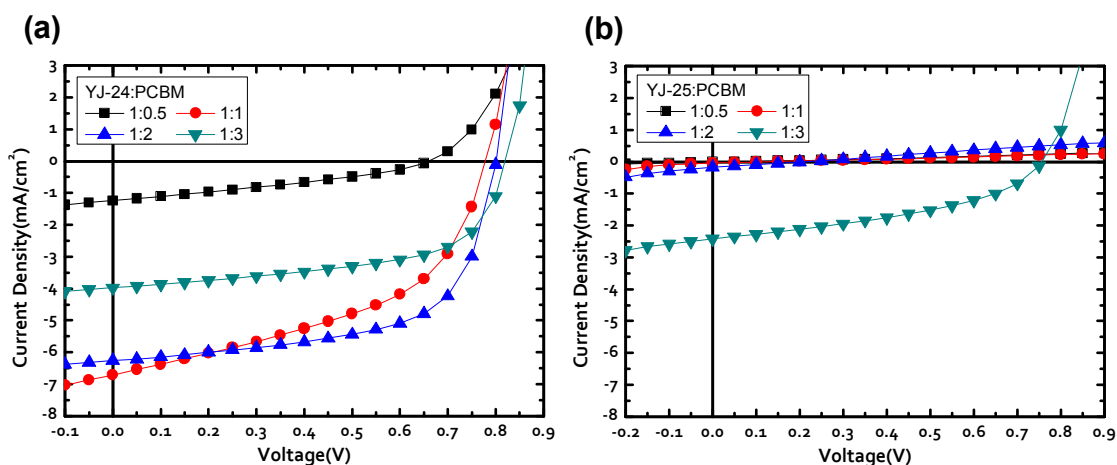


**Figure III-13.** (a) J-V characteristics of the device based on YJ-24:PCBM blend and (b) YJ-25:PCBM blend.

**Table III-7.** Photovoltaic performance of devices based on YJ-24 or YJ-25.

polymer	ratio (polymer:PCBM)	$J_{sc}$ (mA/cm <sup>2</sup> )	$V_{oc}$ (V)	FF	PCE (%)
YJ-24	1 : 0.5	1.24	0.66	0.33	0.27
	1 : 1	6.72	0.79	0.48	2.51
	1 : 2	6.27	0.80	0.62	3.12
	1 : 3	3.97	0.82	0.59	1.91
YJ-25	1 : 0.5	0.005	0.024	0	0
	1 : 1	0.035	0.109	0.227	0.001
	1 : 2	0.177	0.209	0.248	0.009
	1 : 3	2.420	0.756	0.415	0.760

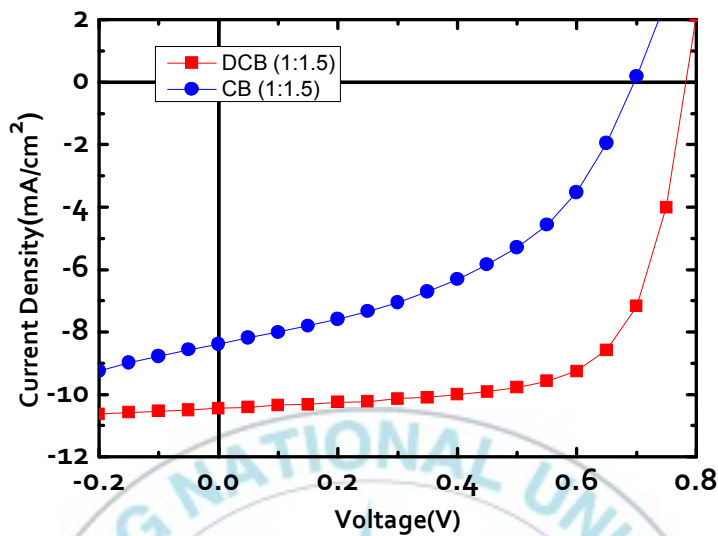


**Figure III-14.** J-V characteristics of the device based on YJ-24:PC<sub>70</sub>BM (1:1.5) blend with 3 vol% DIO.

**Table III-8.** Photovoltaic performance of devices based on YJ-24:PC<sub>70</sub>BM with additive.

YJ-24					
ratio (polymer:PC <sub>70</sub> BM)	solvent (+ 3vol% DIO)	J <sub>sc</sub> (mA/cm <sup>2</sup> )	V <sub>oc</sub> (V)	FF	PCE (%)
1 : 1.5	CB	8.39	0.70	0.45	2.64
	DCB	10.44	0.79	0.68	5.58

### III-5. Film Morphology Analysis

A well-organized bulk heterojunction morphology of the active layer is important for efficient charge dissociation and transport. The surface morphological structure of YJ-24/PC<sub>70</sub>BM blend films using tapping mode AFM are shown in Figure III-15 and Figure III-16. The obtained root-mean-square roughness (RMS) values are 8.98 (without DIO) / 2.03 nm (with DIO) and 1.95 (without DIO) / 2.84 nm (with DIO) for the blend films from CB and DCB solvent, respectively. The phase image of the film from YJ-24 with PC<sub>70</sub>BM using CB and DIO (Figure III-16b) shows minute phase separation compared with using DCB and DIO. It seemed that this morphology did not cause effective charge separation, transport and restrain charge recombination; this may explain the modest FF of 45 %. However, the blend film of YJ-24 and PC<sub>70</sub>BM (Figure III-16d) has a more clear formation of aggregation that exhibits an obviously continuous interpenetrating network. The structure is desired for better charge transport, and thus agrees with the enhanced FF of 68 %.

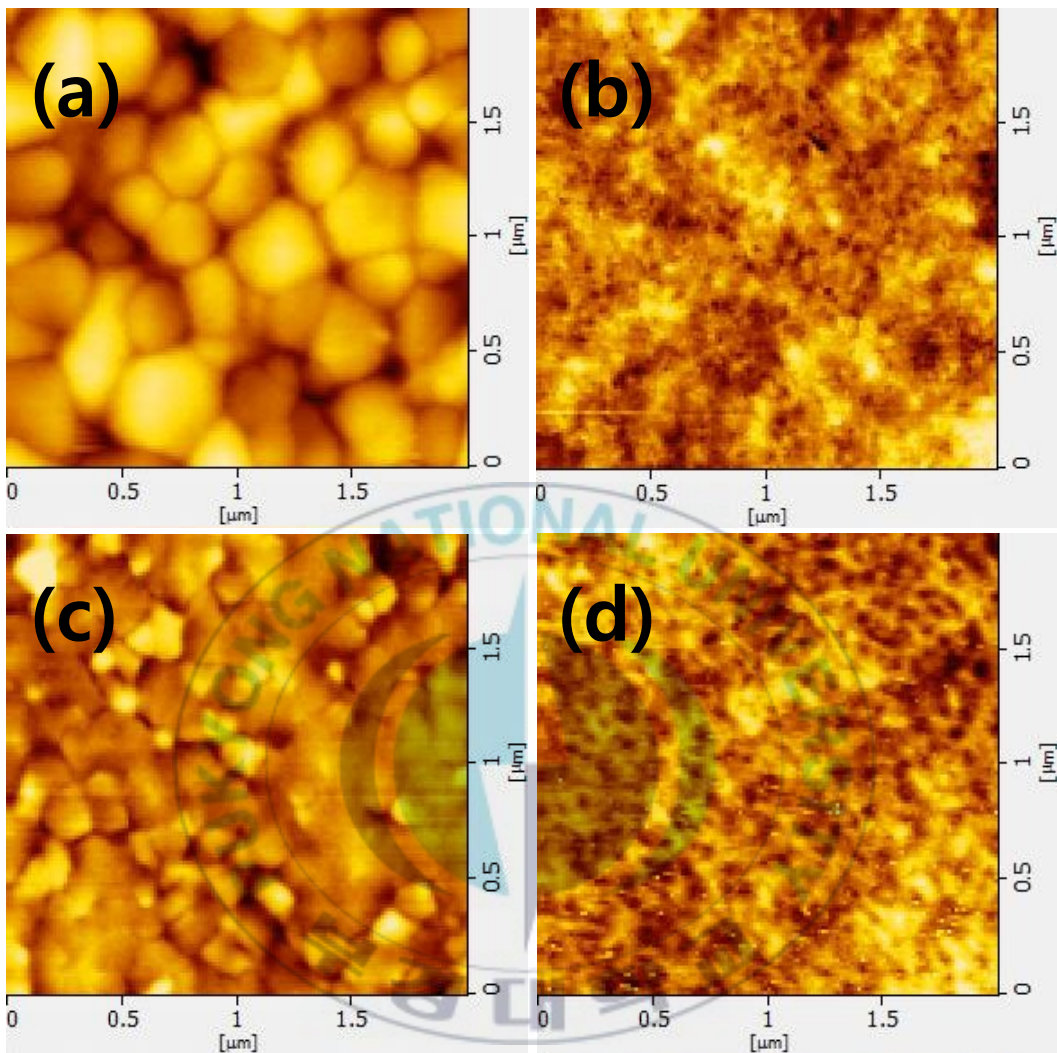


**Figure III-15.** AFM topography images of films spin coated from YJ-24:PC<sub>70</sub>BM (1:2) using chlorobenzene without additives (a) and without DIO (b), using 1,2-dichlorobenzene without additives (c) and with DIO (d). The scan size of the images is 2 μm × 2 μm.

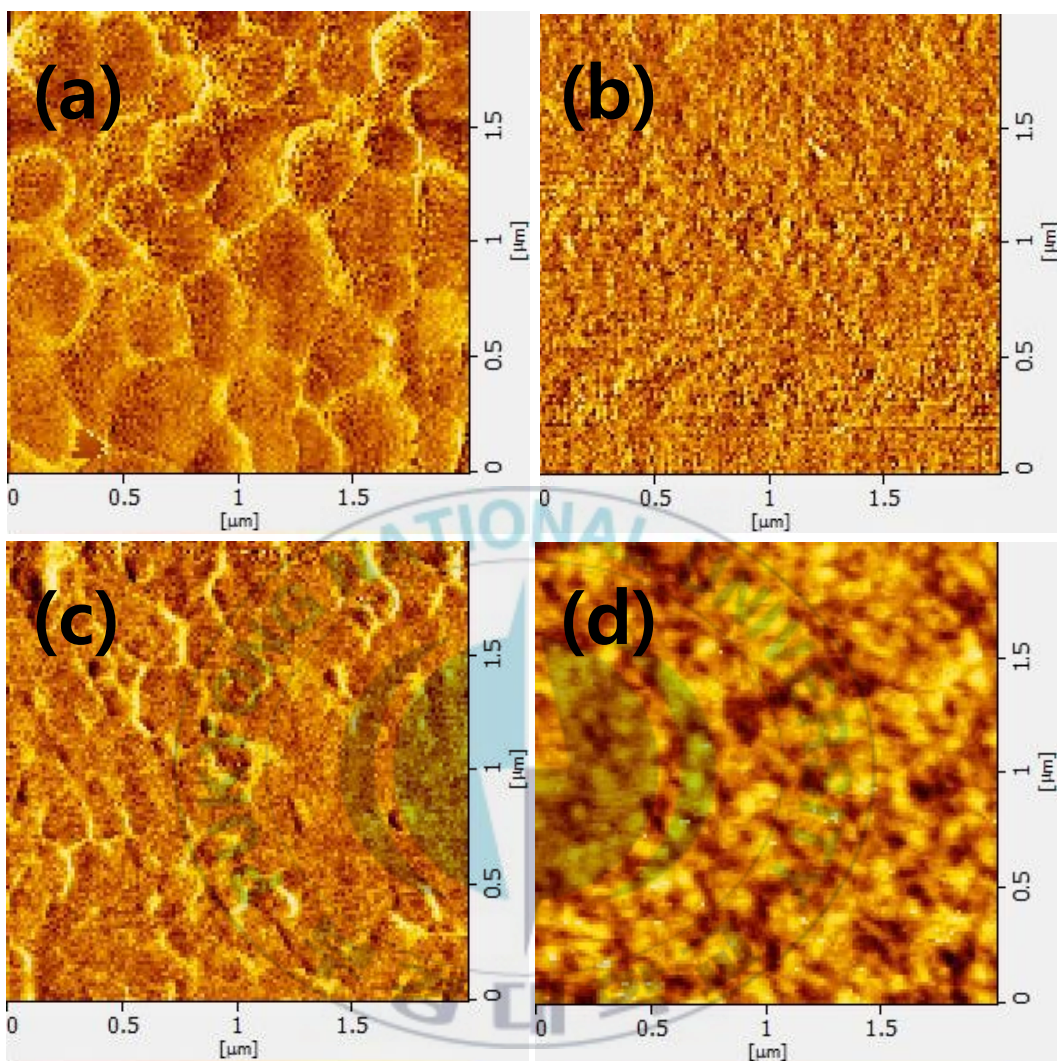


**Figure III-16.** AFM phase images of films spin coated from YJ-24:PC<sub>70</sub>BM (1:2) using chlorobenzene without additives (a) and with DIO (b), using 1,2-dichlorobenzene without additives (c) and with DIO (d). The scan size of the images is 2 μm × 2 μm.

## Chapter IV. Conclusions

In summary, the synthesis of three series polymers containing doubly or singly fluorinated quinoxaline, aiming to invest resulting polymers with favorable properties for the lowering of the polymer HOMO energy levels as well as the creation of the secondary bonding toward further improving the photovoltaic parameters., were named PTDFQ<sub>x</sub>(2F, YJ-20), PTFQ<sub>x</sub>(1F, YJ-21), PBDTDFQ<sub>x</sub>(2F, YJ-22), PBDTFQ<sub>x</sub>(1F, YJ-23), PBDTDTDFQ<sub>x</sub>(2F, YJ-24) and PBDTDTFQ<sub>x</sub>(1F, YJ-25). It seems that the introduction of F atoms into the polymer backbone can fine-tune their energy levels, optical optical properties and molecular packing. The polymers showed desirable deeper HOMO energy levels (-5.39 to -5.69) but the band gaps were of broad width (2.20 to 1.97) because of quite high located LUMO energy levels (-3.40 to -3.57). Among these polymers, the polymers containing one fluorine atom on the backbone showed low-lying HOMO levels compared with polymers containing two fluorine atoms, but their electrochemical bandgaps were slightly lager. As shown in absorption spectra, the optical bandgaps of polymers also had a similar tendency with electrochemical band gaps. When the device performance was measured in all polymers without any processing additives or post treatment at first, PCEs of 1.95, 2.02, 0.49, 0.30, 3.12 and 0.76 % were obtained for YJ-20 ~ YJ-25 based PSCs, respectively. Among these devices, because YJ-24:PCBM = 1:2 device showed the best

performance, additional experiment progressed by changing acceptor and solvent and by adding additive. The experiments performed under condition of YJ-24:PC<sub>70</sub>BM = 1:1.5 ratio, CB or DCB solvent and 3 vol% DIO additive. The device using DCB solvent exhibited the best performance, with a  $V_{oc}$  of 0.79 V,  $J_{sc}$  of 10.44 mA/cm<sup>2</sup>, FF of 0.68 %, PCE of 5.58 %, respectively.

The results shown in this study indicate that the successful application of F atoms to any conjugated polymer for BHJ solar cells can only be realized only with a truly optimized morphology that varies from one polymer/fullerene system to the other. Though investigations to further understand the impact of the F atoms on the morphology, self-assembly behavior, and exciton-related dynamics are currently underway, it is still believed that the triumph morphology remains on the top of research priorities for highly efficient BHJ systems.

## References

- [1] J. J. M. Halls, K. Pichler, R. H. Friend, S. C. Moratti, A. B. Holmes, Appl. Phys. Lett. 68, 3120 (1996)
- [2] M. Theander, A. Yartsev, D. Zigmantas, V. Sundström, W. Mammo, M. R. Andersson, O. Inganäs, Phys. Rev. B 61, 12957 (2000)
- [3] A. Haugeneder, M. Neges, C. Kallinger, W. Spirkl, U. Lemmer, J. Feldmann, U. Scherf, E. Harth, A. Gügel, K. Müllen, Phys. Rev. B 59, 15346 (1999)
- [4] T. Stübinger, W. J. Brütting, Appl. Phys. 90, 3632 (2001)
- [5] D. E. Markov, E. Amsterdam, P. W. M. Blom, A. B. Sieval, J. C. Hummelen, J., Phys. Chem. A 109, 5266 (2005)
- [6] C. W. Tang, Appl. Phys. Lett., 48, 183 (1986)
- [7] T. T. Tsuzuki, J. Shirota, J. Rostalski, D. Meissner, Sol. Energy Mater. Sol. Cells 61, 1 (2000)
- [8] J. X. Uchida, B. P. Rand, S. R. Forrest, Appl. Phys. Lett. 84, 4218 (2004)
- [9] X. Zhou, J. Blochwitz, M. Pfeiffer, A. Nollau, T. Fritz, K. Leo, Adv. Funct. Mater. 11, 310 (2001)
- [10] D. Würhle, D. Meissner, Adv. Mater. 3, 129 (1991)
- [11] S. A. Jenekhe, S. Yi, Appl. Phys. Lett. 77, 2635 (2000)
- [12] A. J. Breeze, A. Salomon, D. S. Ginley, B. A. Gregg, H. Tillmann, H. H.

- Hoerhold, Appl. Phys. Lett. 81, 3085 (2002)
- [13] N. S. Sariciftci, D. Braun, C. Zhang, V. I. Srdanov, A. J. Heeger, G. Stucky, F. Wudl, Appl. Phys. Lett. 62, 585 (1993)
- [14] J. J. M. Halls, C. A. Walsh, N. C. Greenham, E. A. Marseglia, R. H. Friend, S. C. Moratti, A. B. Holmes, Nature 380, 451 (1995)
- [15] C. Winder, N. S. Sariciftci, J. Mater. Chem. 14, 1077 (2004)
- [16] M. G. Harrison, J. Gruener, G. C. W. Spencer, Phys. Rev. B 55, 7831 (1997)
- [17] L. A. A. Petterson, L. S. Roman, O. J. Inganas, Appl. Phys. 86, 487 (1999)
- [18] J. Rotalsky, D. Meissner, Sol. Energy Mater. Sol. Cells 63, 37 (2000)
- [19] H. Hoppe, N. S., J. Sariciftci, Mater. Chem. 19, 1924 (2004)
- [20] J. Hoppe, Ph.D. Thesis, Linz, (2004)
- [21] D. Gebeyehu, B. Maening, J. Drechsel, K. Leo, M. Pfeiffer, Sol. Energy Mater. Sol. Cells 79, 81 (2003)
- [22] M. Hiramoto, H. Fujiwara, M. Yokoyama, Appl. Phys. Lett. 58, 1061 (1991)
- [23] W. Geens, T. Aernouts, J. Poortmans, G. Hadziioannou, Thin Solid Films 403-404, 438 (2002)
- [24] P. Peumans, S. Uchida, S. Forrest, Nature 425, 158 (2003)
- [25] G. Yu, A. J. Heeger, J. Appl. Phys. 78, 4510 (1998)
- [26] C. Y. Yang, A. J. Heeger, Synth. Met. 83, 85 (1996)
- [27] J. J. Dittmer, E. A. Marseglia, R. H. Friend, Adv. Mater. 12, 1270 (2000)
- [28] K. Petritsch, J. J. Dittmer, E. A. Marseglia, R. H. Friend, A. Lux, G. G.

- Rozenberg, S. C. Moratti, A. B. Holmes, *Sol. Energy Mater. Sol. Cells* 61, 63 (2000)
- [29] L. S. Mende, A. Fechtenkoetter, K. Müllen, E. Moons, R. H. Friend, J. D. Mackenzie, *Science* 293, 1119 (2001)
- [30] F. Padinger, R. Rittberger, N. S. Sariciftci, *Adv. Funct. Mater.* 13, 85 (2003)
- [31] M. C. Scharber, D. Mühlbacher, M. Koppe, P. Denk, C. Waldauf, A. J. Heeger, C. Brabec, *J. Adv. Mater.* 18 (6), 789-794 (2006)
- [32] M. D. Perez, C. Borek, S. R. Forrest, M. E. Thompson, *J. Am. Chem. Soc.* 131 (26), 9281-9286 (2009)
- [33] K. Vandewal, K. Tvingstedt, A. Gadisa, O. Inganas, J. V. Manca, *Nature Mater.* 8 (11), 904-909 (2009)
- [34] L. Yang, H. Zhou, W. You, *J. Phys. Chem. C* 114 (39), 16793-16800 (2010)
- [35] A. Moliton, J.-M. Nunzi, *Polym. Int.* 55 (6), 583-600 (2006)
- [36] B. C. Thompson, J. M. Fréchet, *J. Angew. Chem. Int. Ed.* 47 (1), 58-77 (2008)
- [37] R. Kroon, M. Lenes, J. C. Hummelen, P. W. M. Blom, B. de Boer, *Polym. Rev. (Philadelphia, PA, U. S.)* 48 (3), 531-582 (2008)
- [38] H. Zhou, L. Yang, A. C. Stuart, S. C. Price, S. Liu and W. You, *Angew. Chem., Int. Ed.*, 50, 2995-2998 (2011)
- [39] S. C. Price, A. C. Stuart, L. Q. Yang, H. X. Zhou and W. You, *J. Am. Chem. Soc.*, 133, 4625-4631 (2011)

- [40] C. M. Amb, S. Chen, K. R. Graham, J. Subbiah, C. E. Small, F. So and J. R. Reynolds, *J. Am. Chem. Soc.*, 133, 10062-10065 (2011)
- [41] T.-Y. Chu, J. Lu, S. Beaupre, Y. Zhang, J.-R. Pouliot, S. Wakim, J. Zhou, M. Leclerc, Z. Li, J. Ding and Y. Tao, *J. Am. Chem. Soc.*, 133, 4250-4253 (2011)
- [42] C. E. Small, S. Chen, J. Subbiah, C. M. Amb, S.-W. Tsang, T.-H. Lai, J. R. Reynolds and F. So, *Nat. Photonics*, 6, 115-120 (2011)
- [43] Y. Y. Liang, Y. Wu, D. Q. Feng, S. T. Tsai, H. J. Son, G. Li and L. P. Yu, *J. Am. Chem. Soc.*, 131, 56-57 (2009)
- [44] Y. Huang, L. Huo, S. Zhang, X. Guo, C. C. Han, Y. Li and J. Hou, *Chem. Commun.*, 47, 8904-8906 (2011)
- [45] Z. He, C. Zhong, X. Huang, W.-Y. Wong, H. Wu, L. Chen, S. Su and Y. Cao, *Adv. Mater.*, 23, 4636-4643 (2011)
- [46] L. Huo, J. Hou, S. Zhang, H.-Y. Chen, Y. Yang, *Angew. Chem., Int. Ed.*, 49 (8), 1500-1503 (2010)
- [47] H. Zhou, L. Yang, A. C. Stuart, S. C. Price, S. Liu, W. You, *Angew. Chem., Int. Ed.*, 50 (13), 2995-2998 (2011)
- [48] H. Zhou, L. Yang, S. C. Price, K. J. Knight, W. You, *Angew. Chem., Int. Ed.*, 49 (43), 7992-7995 (2010)
- [49] R. J. Kline, M. D. McGehee, E. N. Kadnikova, J. Liu, J. M. J. Fréchet, M. F. Toney, *Macromolecules*, 38 (8), 3312- 3319 (2005)

- [50] H. Zhou, L. Yang, S. Xiao, S. Liu, W. You, *Macromolecules*, 43 (2), 811-820 (2010)
- [51] X. Wang, E. Perzon, W. Mammo, F. Oswald, S. Admassie, N.-K. Persson, F. Langa, M. R. Andersson, O. Inganaes, *Thin Solid Films*, 511-512 (1), 576-580 (2006)
- [52] J.-H. Tsai, C.-C. Chueh, M.-H. Lai, C.-F. Wang, W.-C. Chen, B.-T. Ko, C. Ting, *Macromolecules*, 42 (6), 1897-1905 (2009)
- [53] S. Sadki, P. Schottland, N. Brodie, G. Sabouraud, *Chem. Soc. Rev.*, 29, 283 (2000)
- [54] J. Roncali, *Chem. Rev.* 92, 711 (1992)
- [55] R. J. Waltman, J. Bargon, *Can. J. Chem.* 64, 76 (1986)
- [56] N. Toshima, S. Hara, *Prog. Polym. Sci.* 20, 155 (1995)
- [57] Y.-J. Cheng, T.-Y. Luh, *J. Organomet. Chem.* 689, 4137 (2004)
- [58] K. Tamao, K. Sumitani, M. Kumda, *J. Am. Chem. Soc.* 94, 4374 (1972)
- [59] J. K. Stille, *Angew. Chem. Int. Ed.* 25, 508 (1986)
- [60] N. Miyaura, A. Suzuki, *Chem. Rev.* 95, 2457 (1995)
- [61] K. Sonogashira, *J. Organomet. Chem.* 653, 46 (2002)
- [62] Z. Bao, W. K. Chan, L. Yu, *J. Am. Chem. Soc.* 117, 12426 (1995)
- [63] T. Yamamoto, A. Morita, Y. Miyazaki, T. Maruyama, H. Wakayama, Z.-H. Zhou, Y. Nakamura, T. Kanbara, S. Sasaki, K. Kubota, *Macromolecules* 25,

1214 (1992)

- [64] Jonggi Kim, Myoung Hee Yun, Gi-Hwan Kim, Jungho Lee, Sang Myeon Lee, Seo-Jin Ko, Yiho Kim, Gitish K. Dutta, Mijin Moon, Song Yi Park, Dong Suk Kim, Jin Young Kim, and Changduk Yang, ACS Appl. Mater. Interfaces, 6, 7523-7534 (2014)

